

Bifrost: A Much Simpler Secure Two-Party Data Join Protocol for Secure Data Analytics

Shuyu Chen

Fudan University

23110240005@m.fudan.edu.cn

Mingxun Zhou

The Hong Kong University of Science
and Technology

mingxunz@ust.hk

Haoyu Niu

Fudan University

23212010019@m.fudan.edu.cn

Guopeng Lin

Fudan University

17302010022@m.fudan.edu.cn

Weili Han

Fudan University

wlhan@m.fudan.edu.cn

ABSTRACT

Secure data join enables two parties with vertically distributed data to securely compute the joined table, allowing the parties to perform downstream Secure multi-party computation-based Data Analytics (SDA), such as analyzing statistical information or training machine learning models, based on the joined table. While Circuit-based Private Set Intersection (CPSI) can be used for secure data join, it inherently introduces redundant dummy rows in the joined table on top of the actual matched rows, which results in high overhead in the downstream SDA tasks. iPrivJoin addresses this issue but introduces significant communication overhead in the redundancy removal process, as it relies on the cryptographic primitive Oblivious Programmable Pseudorandom Function (OPPRF) and multiple rounds of oblivious shuffles.

In this paper, we propose a much simpler secure data join protocol, Bifrost, which outputs (the secret shares of) a redundancy-free joined table. The highlight of Bifrost lies in its simplicity: it builds upon two conceptually simple building blocks, an ECDH-PSI protocol and a two-party oblivious shuffle protocol. The lightweight protocol design allows Bifrost to avoid the need for OPPRF. We also proposed a simple optimization named *dual mapping* that reduces the rounds of oblivious shuffle needed from two to one. Experiments on various datasets up to 100 GB show that Bifrost achieves $2.54 \sim 22.32 \times$ speedup and reduces the communication by $84.15\% \sim 88.97\%$ compared to the state-of-the-art redundancy-free secure data join protocol iPrivJoin. In addition, the communication size of Bifrost is nearly equal to the size of the input data. In the experiments involving the entire two-step SDA pipeline (secure join and secure analytics), the redundancy-free property of Bifrost not only avoids the catastrophic error rate blowup in the downstream tasks caused by the dummy padded outputs in the secure joined table (as introduced in CPSI), but also shows up to $2.80 \times$ speed-up in the secure analytics process with up to 73.15% communication reduction.

PVLDB Reference Format:

Shuyu Chen, Mingxun Zhou, Haoyu Niu, Guopeng Lin, and Weili Han. Bifrost: A Much Simpler Secure Two-Party Data Join Protocol for Secure Data Analytics. PVLDB, 19(6): XXX-XXX, 2026.
doi:XX.XX/XXX.XX

This work is licensed under the Creative Commons BY-NC-ND 4.0 International License. Visit <https://creativecommons.org/licenses/by-nc-nd/4.0/> to view a copy of this license. For any use beyond those covered by this license, obtain permission by emailing info@vldb.org. Copyright is held by the owner/author(s). Publication rights

PVLDB Artifact Availability:

The source code, data, and/or other artifacts have been made available at: <https://github.com/stellasuc/secdjoin.git>

1 INTRODUCTION

Secure Multi-Party Computation (SMPC) enables multiple parties to jointly compute some functions over their data while keeping their data private. By leveraging SMPC, parties can perform various Secure Data Analytics (SDA) tasks, including performing statistical analysis on their distributed data or even training a machine learning model, which helps address privacy-related data compliance requirements, such as GDPR [64] and CCPA [8].

Vertically distributed data is a common setting in real-world SDA applications, appearing in many privacy-critical scenarios, including finance [13, 27], e-commerce [12, 65], and healthcare [5, 66]. That is, the parties' data tables overlap in the indexing IDs but have disjoint feature columns (see Figure 1). For example, consider a hospital that is cooperating with a genomic research company on training a cancer risk assessment model based on genetic data. The hospital holds the health record table of its patients, and the genomic research company holds the gene description table of its clients. Both tables are indexed by the individuals' unique IDs. They will need to first *align* the data by the IDs and build a training dataset that contains only the records of those individuals who appear in both original tables. In the traditional setting with no privacy constraint, the parties can run a classical distributed *join* operation [9, 32, 54] on the tables and obtain a joined table that cross-matches the records in the original tables based on IDs and concatenates the feature columns. They can then proceed to train their models based on the data samples in this joined table.

In our targeted privacy-constrained setting, a *secure join* protocol is required instead of a traditional distributed join algorithm, given that these algorithms inherently leak sensitive information about one party's data table to the other party. The secure join protocol ensures that the computation process of the join operation reveals only the absolutely necessary information to both parties (e.g., the size of the final joined table), and outputs the joined table in secret-shared form to both parties, so neither party learns the full, privacy-sensitive joined table.

licensed to the VLDB Endowment.

Proceedings of the VLDB Endowment, Vol. 19, No. 6 ISSN 2150-8097.

doi:XX.XX/XXX.XX

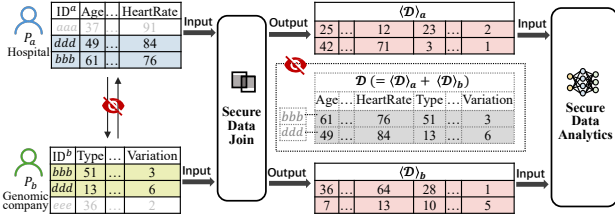


Figure 1: An example of a vertically distributed data setting. P_a and P_b each hold a table with three records. Both tables contain the intersection IDs “bbb” and “ddd”.

Existing secure data join schemes either introduce significant computation and/or communication costs, or pass down nonideal overhead to the downstream SDA tasks. On the one hand, Circuit-based Private Set Intersection (CPSI) [52, 53] can be used for secure data join, but the protocols will inherently introduce many redundant dummy rows in the joined table (padded to the maximum length) other than the actual matched rows, which could be a huge waste in many practical scenarios. Liu *et al.* [40] showed that the redundant rows generated by CPSI may cause both downstream SDA tasks’ time and communication overhead to increase by up to $3\times$, and proposed another state-of-the-art (SOTA) secure data join method named iPrivJoin. However, to remove the redundant rows, iPrivJoin introduces excessive communication overhead in the secure data join process, which stems from its reliance on Oblivious Programmable Pseudorandom Function (OPPRF) [53] for data encoding and two rounds of oblivious shuffle. Apart from that, iPrivJoin also requires 11 rounds of communication between the two parties, becoming another disadvantage for its practicality. Our experiments show that for the table size of 100 GB under WAN setting, iPrivJoin requires 53.87 hours in time cost and 773.95 GB in communication cost.

As a versatile building block, a secure join protocol can be applied to secure data mining [2, 38], SQL operators [6, 62], and data visualizations [4, 48] applications, in addition to the aforementioned SDA tasks. Given the importance of an efficient secure join protocol in these applications, we ask the following question:

How to construct a redundancy-free secure data join protocol with high computation efficiency and low communication cost?

1.1 Our Contributions

In this paper, we propose Bifrost, a conceptually simple secure data join protocol with better performance compared to the baselines. We summarize our main contributions as follows:

- We propose a new secure two-party data join protocol named Bifrost that outputs (the secret shares of) the redundancy-free joined table. The highlight of Bifrost lies in its simplicity: Bifrost builds upon two conceptually simple building blocks, an Elliptic-Curve-Diffie-Hellman-based Private Set Intersection (ECDH-PSI) protocol [29, 44] and a two-party oblivious shuffle protocol [40]. The lightweight protocol design allows Bifrost to avoid many performance bottlenecks in iPrivJoin, including the need for Cuckoo hashing and OPPRF. We also propose a simple optimization named *dual mapping* that reduces the rounds of oblivious shuffle (as in iPrivJoin) needed from two to one.

- We provide a theoretical analysis of Bifrost’s asymptotic performance and show that it outperforms the baselines in nearly all important metrics, including computation, communication, and round complexities. We also provide the rigorous security proof for Bifrost to meet the privacy requirement.
- We extensively evaluate the effectiveness of Bifrost in the pipeline of SDA tasks, including secure statistical analysis and secure training. First, we show that our redundancy-free design of Bifrost allows the downstream SDA tasks to achieve high-accuracy outputs, avoiding the catastrophic error rate blowup caused by CPSI-based solution [52, 53]. Moreover, the design helps the downstream SDA tasks achieve up to $2.80\times$ improvement in running time with up to 73.09% less communication compared to pipelines using CPSI.
- We empirically evaluate Bifrost on various datasets up to 100 GB and compare its performance against the baselines. We show that, on real-world datasets, Bifrost achieves up to $15.2\times$ and up to $10.36\times$ speedups compared to iPrivJoin [40] and CPSI [52], respectively. In addition, compared to the redundancy-free secure data join baseline iPrivJoin, Bifrost achieves $2.54 \sim 22.32\times$ faster running time and reduces communication size by 84.15% \sim 88.97%. Moreover, the advantages of Bifrost become more pronounced as the feature dimension increases. For instance, when the feature dimension varies from 100 to 6400, the running time improvement increases from $9.58\times$ to $21.46\times$. Notably, the communication size of Bifrost is nearly equal to the size of the input data.

1.2 Design Goal and Technical Overview

Design Goal. We aim to design a secure two-party data join protocol, Bifrost. To clarify this goal, we first define the two-party data join operation [6, 51]. Consider two tables, T_a and T_b , held by two parties P_a and P_b , respectively. Each table consists of identifiers and corresponding feature columns. A two-party data join operation inputs T_a and T_b and outputs a joined table \mathcal{D} by identifying the matched identifiers across both tables and concatenating their respective feature columns. This join operation can be expressed in SQL as follows:

```
SELECT Ta.* EXCEPT (identifiers), Tb.* EXCEPT (identifiers)
FROM Ta JOIN Tb
ON Ta.identifiers = Tb.identifiers
```

The *secure* two-party data join protocol, Bifrost, ensures that this join operation is performed securely. Here, “secure” means that Bifrost reveals only the size of the joined table during the computation process of the join operation, and outputs (secret) shares of the joined table to both parties (one share per party). Note that each joined table share is uniformly random, so it reveals nothing about the joined table value or the matched identifiers. Furthermore, these shares enable the two parties to directly perform downstream secure data analytics on the joined table shares using secure multi-party computation techniques.

Simplified Setting Description. To show how Bifrost achieves this design goal, we now provide a technical overview in a simplified setting. There are two tables consisting of identifiers and the corresponding feature columns, $[(ID_i^a, F_i^a)]_{i \in [n]}$ and $[(ID_i^b, F_i^b)]_{i \in [n]}$,

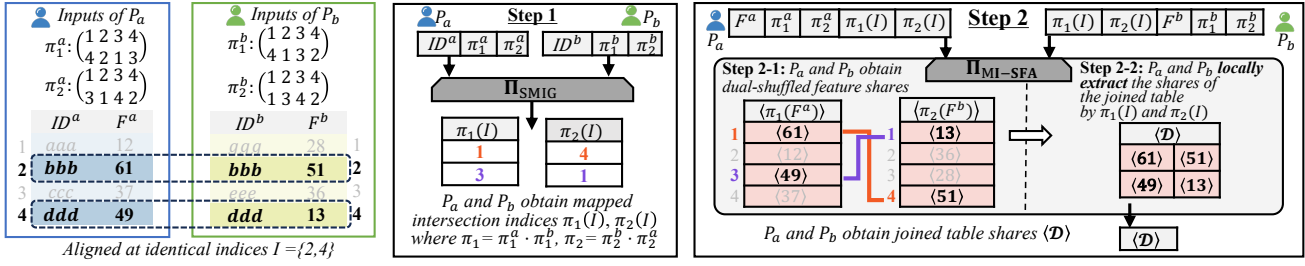


Figure 2: Simplified workflow of Bifrost with *Dual Mapping* optimization. The intersection IDs and their features are highlighted in bold. In the first step, both parties obtain mapped intersection indices $\pi_1(I)$ and $\pi_2(I)$. In the second step, both parties first obtain dual-shuffled feature shares $\langle \pi_1(F^a) \rangle$ and $\langle \pi_2(F^b) \rangle$ via one round of $\Pi_{O\text{-Shuffle}}$, then both parties locally extract the shares of the joined table \mathcal{D} from $\langle \pi_1(F^a) \rangle$ and $\langle \pi_2(F^b) \rangle$ according to $\pi_1(I)$ and $\pi_2(I)$.

held by party P_a and P_b , respectively. Both parties want to run some downstream task on the *joined table*, that is, $\{(F_i^a, F_i^b)\}_{i \in I}$ where the list I includes all matched indices: $I = [i \mid ID_i^a = ID_i^b]$. We focus on designing an interactive protocol between the parties that outputs secret shares of the joined table to both parties (one share per party) without exposing the intersection index set I to either party.

For simplicity, we make the assumption here that the tables are “aligned”, i.e., if an identifier appears in both tables, the corresponding rows must share the same relative location in the lists. This “aligned” simplicity allows us to focus on the challenge of how to identify I and extract the corresponding feature pairs $\{(F_i^a, F_i^b)\}_{i \in I}$ in secret-shared form without revealing I itself. The unaligned case, which is typically the standard definition of the secure join problem, can be accommodated through protocol-specific modifications.

Workflow of Bifrost. The two major steps are:

- (1) *Secure mapped intersection generation (SMIG)*. In this step, the two parties obliviously find all the matched indices I where $ID_i^a = ID_i^b$ for $i \in I$. For privacy, neither party can learn the indices I directly. Instead, our proposed protocol outputs a *mapped* version of the matched indices I , denoted as $\pi(I)$, where $\pi : [n] \mapsto [n]$ is a mapping (shuffling) unknown to both parties. We set π as the composition of two shuffles π^a, π^b , each only known to party P_a and P_b respectively. This ensures that both parties learn only the size of the intersection (i.e., row count of the joined table) and nothing else. To securely instantiate this step, we adapt an Elliptic-Curve-Diffie-Hellman-based Private Set Intersection (ECDH-PSI) protocol [29, 44] to our setting with several technical changes.
- (2) *Secure feature alignment*. The second step is straightforward: the parties jointly run an oblivious shuffling protocol [40] to obtain the shares of $\pi(F^a)$ and $\pi(F^b)$ ¹. Then, both parties can locally extract the shares of the joined table. That is, they collect the shares of $\{(\pi(F^a)_i, \pi(F^b)_i)\}_{i \in \pi(I)}$, which is exactly $\{(F_i^a, F_i^b)\}_{i \in I}$.

Example: the two parties hold $[(aaa, 12), (bbb, 61), (ccc, 37), (ddd, 49)]$ and $[(ggg, 28), (bbb, 51), (eee, 36), (ddd, 13)]$, respectively. The matched indices are $I = [2, 4]$, corresponding to the intersection identifiers “bbb” and “ddd”. Given a shuffle $\pi : (1 \rightarrow 3, 2 \rightarrow 1, 3 \rightarrow$

4, 4 \rightarrow 2) unknown to both parties, the secure mapped intersection generation protocol outputs the mapped intersection indices $\pi(I) = \pi([2, 4]) = [1, 2]$. Then, both parties run the oblivious shuffle protocol [40] to shuffle their local feature columns according to π and obtain the shares of the two shuffled feature columns: [61, 49, 12, 37] and [51, 13, 28, 36]. Now, given the mapped intersection indices [1, 2], they simply collect the first and the second entries in the local shares, which are the shares of the concatenated intersection features: [(61, 51), (49, 13)].

Optimization: Dual Mapping. A performance bottleneck of the aforementioned workflow is the secure shuffle protocol in the second step. The two-party oblivious shuffle protocol $\Pi_{O\text{-Shuffle}}$ [40] is designed for the following functionality: given the input of a data column (from one party) and a shuffle (from another party), the protocol outputs the shares of the shuffled data column to both parties. Recall that the shuffle π is a composition of π^a and π^b (first applying π^a , then applying π^b). When the parties run the oblivious shuffle protocol to shuffle the feature columns of F^a , P_a can first locally shuffle the feature columns according to π^a . Then, they can directly call $\Pi_{O\text{-Shuffle}}$ given the self-shuffled features $\pi^a(F^a)$ from P_a and the shuffle π^b from P_b to obtain the share of $\pi(F^a)$. However, when they need to shuffle the column of F^b , P_b cannot shuffle the column locally according to π^b first, because the shuffling operation is not commutative (i.e., $\pi = \pi^a \circ \pi^b$ may not be the same as $\pi^b \circ \pi^a$). A naive solution could be running the $\Pi_{O\text{-Shuffle}}$ twice, resulting in high communication overhead.

We propose a simple yet effective optimization called *Dual Mapping* to address this issue. That is, we now modify the secure mapped intersection generation (SMIG) protocol to output *two* mapped versions of the intersection indices I with two different mappings, π_1 and π_2 . Importantly, we let $\pi_1 = \pi_1^a \circ \pi_1^b$ and $\pi_2 = \pi_2^b \circ \pi_2^a$ where π_1^a, π_2^a are only known to P_a , and π_1^b, π_2^b are only known to P_b . Then, in the oblivious shuffle protocol execution later, P_a ’s feature columns will be shuffled by π_1 , while P_b ’s feature columns will be shuffled by π_2 . A simplified workflow of Bifrost with the *Dual Mapping* optimization is shown in Figure 2. The advantage is that now both first layers of the shuffles can be done by the corresponding party locally, and we only need to execute the oblivious shuffle protocol once on both sides. Effectively, this optimization saves $O(m_b)$ online communication overhead compared to the naive solution, where m_b denotes the feature dimension for P_b .

¹We abuse the notation here that $\pi(F^a)_{\pi(i)} = F_i^a$ for all $i \in [n]$.

Supporting the General Scenario. In practice, the tables from both parties are usually not aligned, i.e., the rows with the same identifier may not be in the same relative location in the two tables. The prior standard solutions to this issue, including CPSI [52] and iPrivJoin [40], use a combination of Cuckoo hashing [50] and simple hashing to place the data elements in the same relative location in the hash tables. This further complicates the protocol design and affects the overall performance.

Instead, our protocol is naturally capable of handling the general scenario without requiring any hashing technique involved, saving another $O(hm_b\kappa)$ in computation cost and $O(hm_b\kappa)$ in communication cost, where κ is the computational security parameter and h is the number of hashing functions. More specifically, our protocol simply outputs the mapped intersection index pairs MIPairs = $\{(\pi_1(i), \pi_2(j)) \mid ID_i^a = ID_j^b\}$ in the first step, and proceeds as before. We demonstrate that this upgrade can be implemented with a minor modification to our aforementioned ECDH-PSI-based [44] secure mapped intersection generation protocol, incurring no additional overhead.

Comparison with the Prior State-of-the-art Scheme. Compared to the prior best scheme iPrivJoin, our proposed Bifrost achieves significantly better efficiency in terms of communication and computation overhead by fundamentally restructuring the workflow. Specifically, iPrivJoin operates in three steps: (1) private data encoding: the parties use Cuckoo hashing or simple hashing tables for data allocation and OPPRF [34] for data encoding, obtaining shares of (B, F^a, F^b) with $B_i = 0$ for intersection rows and a random value otherwise; (2) oblivious shuffle: the two parties employ two rounds of an oblivious shuffle protocol on encoded data to obtain shares of $\pi(B, F^a, F^b)$. Here, π is the composite of two shuffles π^a, π^b , each only known to P_a and P_b , respectively. (3) private data trimming: the two parties reconstruct $\pi(B)$ in plaintext and remove redundant rows from shares of $\pi(F^a, F^b)$ according to $\pi(B)$. The bottlenecks in iPrivJoin are twofold: Firstly, in the first step, all data from the two parties must be communicated, particularly through OPPRF, incurring both communication and computational complexities of $O(hn(\lambda + \log n + m_b\kappa) + nm_a\ell)$. Here λ and κ are security parameters, ℓ is the element bit length, and h is the number of hash functions. Secondly, in the second step, two rounds of $\Pi_{O\text{-}Shuffle}$ on encoded data are required due to the secret-shared nature of the encoded data, incurring both communication and computation complexities of $2n(m_a\ell + m_b\ell + \kappa)$.

In contrast, Bifrost builds upon two conceptually simple building blocks, an ECDH-PSI protocol [29, 44] and the oblivious shuffle protocol [40], eliminating Cuckoo hashing and OPPRF. Notably, ECDH-PSI overhead $O(n\sigma)$ (where σ is the ECC key bit-length), depends only on identifiers and not on feature dimensions. We further propose a simple optimization named *dual mapping* that reduces the need for two rounds of oblivious shuffle (as in iPrivJoin) to one round. As a result, the total communication and computation complexity of Bifrost are both $O(n\sigma + nm_a\ell + nm_b\ell)$, reducing overhead by at least 66.7% compared to iPrivJoin. As shown in Table 1, Bifrost exhibits substantially lower online communication overhead than iPrivJoin. Moreover, Bifrost reduces offline communication at least by half compared to iPrivJoin. A more detailed communication comparison is provided in Appendix C.

Table 1: Comparison of Bifrost and iPrivJoin [40] in online communication. Here, n is the row count of the input data; m_a and m_b are the feature dimensions for P_a and P_b , respectively; $m = m_a + m_b$; ℓ is the element bit length; σ is the ECC key bit length; h is the number of hash functions; λ and κ are the statistical security parameter and the computational security parameter, respectively.

Protocol	Communication Size (bits)		Round
	Step (1)	Step (2)+(3)	
iPrivJoin [40]	$O(hn(\lambda + \log n + m_b\kappa) + nm_a\ell)$	$O(nm\ell + nk)$	11
Bifrost	$O(n\sigma + nm\ell)$		4

2 PRELIMINARIES

Notations. We use the notation $\{x_1, \dots, x_t\}$ to denote an unordered set and the notation $[x_1, \dots, x_t]$ to denote an ordered list.

ECDH-PSI. Private Set Intersection (PSI) protocols constructed using Elliptic Curve Cryptography (ECC) [33, 45] are commonly referred to as ECDH-PSI [29, 44]. ECC is typically preferred in PSI because it offers the same security level with significantly smaller key sizes compared to other cryptographic algorithms with similar functionality, such as RSA. Technically, ECC relies on the algebraic properties of elliptic curves over finite fields. An elliptic curve E over \mathbb{Z}_q is defined by the equation $y^2 = x^3 + \gamma_1x + \gamma_2 \pmod{q}$, where $\gamma_1, \gamma_2 \in \mathbb{F}_q$ satisfy the non-singularity condition $4\gamma_1^3 + 27\gamma_2^2 \not\equiv 0 \pmod{q}$. Scalar multiplication on this curve, denoted as kQ , represents the repeated addition of a point Q to itself k times. The security of ECC is based on the hardness of the elliptic curve discrete logarithm problem (ECDLP) [24]: given two points Q and $Q_2 = kQ$, it is computationally infeasible to recover k .

In a typical ECDH-PSI protocol, two parties P_a and P_b hold data $X = [x_i]_{i \in [n]}$ and $Y = [y_i]_{i \in [n]}$, respectively. They first map their input data to points on an elliptic curve using a cryptographic hash function $H(\cdot)$. Then, they compute the intersection set as follows:

- (1) P_a and P_b each generates a private scalar key, denoted α and β , respectively.
- (2) P_b computes $\beta Y = [\beta H(y)]_{y \in Y}$ and sends βY to P_a .
- (3) P_a shuffles its data to obtain $\pi(X)$ and computes $\alpha\pi(X) = [\alpha H(x)]_{x \in \pi(X)}$. P_a receives βY and computes $\alpha\beta Y = [\alpha y]_{y \in \beta Y}$. P_a sends $\alpha\pi(X)$ and $\alpha\beta Y$ to P_b .
- (4) Upon receiving $\alpha\pi(X)$ and $\alpha\beta Y$, P_b computes $\beta\alpha\pi(X) = [\beta x]_{x \in \alpha\pi(X)}$. Since scalar multiplication on elliptic curves is commutative (i.e., $\alpha\beta = \beta\alpha$), P_b finally obtains the intersection set by evaluating $\beta\alpha\pi(X) \cap \alpha\beta Y$. P_b can reveal their intersection elements to P_a if necessary.

Additive Secret Sharing. Additive secret sharing is a key technology in SMPC [18, 68]. In the two-party setting of additive secret sharing, an ℓ -bit value x is split into two secret-shared values (i.e., shares), denoted $\langle x \rangle_a$ and $\langle x \rangle_b$, where $\langle x \rangle_* \in \mathbb{Z}_{2^\ell}$ and each party P_* holds one share $\langle x \rangle_*$ for $*$ $\in \{a, b\}$. The original value x can be revealed by summing all shares: $\langle x \rangle_a + \langle x \rangle_b \equiv x \pmod{2^\ell}$.

Oblivious Shuffle. The oblivious shuffle functionality $\mathcal{F}_{O\text{-}Shuffle}$ inputs a random permutation π from P_b and inputs a matrix X from P_a . It outputs a secret-shared and shuffled matrix $\langle \pi(X) \rangle$ while ensuring that the permutation π is unknown to P_a and X is unknown to P_b . In this paper, we employ the oblivious shuffle

protocol $\Pi_{O\text{-Shuffle}}$ (Protocol 1). In the online phase of Protocol 1, the communication size and round are $n \cdot m$ and 1, respectively, where $n \cdot m$ is the size of matrix X . Additionally, for the offline phase of $\Pi_{O\text{-Shuffle}}$, we employ the protocol in Algorithm 2 in [40].

Protocol 1: $\Pi_{O\text{-Shuffle}}$

Parameters: The size of matrix $n \times m$; The bit length of element ℓ .
Inputs: P_a holds a matrix $X \in \mathbb{Z}_{2^\ell}^{n \times m}$.

Outputs: Each party obtains $\langle \pi(X) \rangle$, where π is only known to P_b .
Offline: P_a generates a random matrix $R \in \mathbb{Z}_{2^\ell}^{n \times m}$. P_b samples a random permutation $\pi : [n] \mapsto [n]$. Then, two parties invoke an instance of $\mathcal{F}_{O\text{-Shuffle}}$ to obtain $\langle \pi(R) \rangle$.

Online:

1. P_a computes $\hat{X} = X - R$ and sends \hat{X} to P_b .
2. P_a sets $\langle \pi(X) \rangle_a = \langle \pi(R) \rangle_a$.
3. P_b computes $\langle \pi(X) \rangle_b = \pi(X) + \langle \pi(R) \rangle_b$.

3 PROBLEM DESCRIPTION

We summarize notations we use in Table 2.

Table 2: Notations used in this paper.

Symbol	Description
P_a, P_b	Two parties involved in secure data join.
n	The row count of the input data.
m_a, m_b	The feature dimension of P_a and P_b , respectively.
m	The total feature dimension ($m = m_a + m_b$).
c	The row count of the joined table.
ID^a, ID^b	The identifiers (IDs) of P_a and P_b , respectively.
F^a, F^b	The features of P_a and P_b , respectively.
\mathcal{D}	The redundancy-free joined table.
$ ID^a \cap ID^b $	The size of the intersection identifiers.
\mathbb{Z}_{2^ℓ}	The ring size used in our paper.
$\mathbb{Z}_{2^\ell}^{c \times m}$	All $c \times m$ matrices whose elements are from the ring \mathbb{Z}_{2^ℓ} .
$\langle x \rangle_*$	The share (i.e., secret-shared value) of x for P_* .
X_i	The i -th element of X .
$X_{i,j}$	The j -th element of i -th row in X .
$\{x_1, \dots, x_t\}$	An unordered set.
$[x_1, \dots, x_t]$	An ordered list.
$[x]$	An ordered list $[1, 2, \dots, x]$.

Problem Definition. To formally define the problem, we present the functionality $\mathcal{F}_{2PC\text{-}DJoin}$ of the secure two-party data join. Note that $\mathcal{F}_{2PC\text{-}DJoin}$ specifies how to realize a secure data join with a third trusted party (TTP), while our proposed **Bifrost** realizes it without such a TTP. As shown in Figure 3, $\mathcal{F}_{2PC\text{-}DJoin}$ inputs (ID^a, F^a) from P_a and inputs (ID^b, F^b) from P_b . Here, ID^* is an ordered list of n identifiers (IDs) and F^* is the corresponding features of size $n \times m_*$ for $*$ $\in \{a, b\}$. $\mathcal{F}_{2PC\text{-}DJoin}$ outputs shares $\langle \mathcal{D} \rangle_a$ and $\langle \mathcal{D} \rangle_b$ of the joined table \mathcal{D} to P_a and P_b , respectively. Specifically, the joined table \mathcal{D} contains $c = |ID^a \cap ID^b|$ rows, where each row consists of m_a features from P_a and m_b features from P_b for an intersection ID. The joined table shares satisfy $\langle \mathcal{D} \rangle_a + \langle \mathcal{D} \rangle_b = \mathcal{D}$ and are sampled uniformly at random. Since each party only obtains a joined table share that is independent of \mathcal{D} , neither party learns the intersection IDs nor the feature values in \mathcal{D} . Consequently, after executing $\mathcal{F}_{2PC\text{-}DJoin}$, neither party learns any extra information beyond what is revealed by the size $c \times m$ of the joined table.

Functionality $\mathcal{F}_{2PC\text{-}DJoin}$

Parameters: The input data row count n . The bit length of element ℓ . P_a 's and P_b 's feature dimensions m_a and m_b . $m = m_a + m_b$.

Input: P_a inputs its data (ID^a, F^a) . P_b inputs its data (ID^b, F^b) .

Functionality:

1. Let intersection identifiers $ID^{a \cap b} = ID^a \cap ID^b$. Define the joined table row count as $c = |ID^{a \cap b}|$.
2. Let joined table $\mathcal{D} = \{[F_{j_a, 1}^a, \dots, F_{j_a, m_a}^a, F_{j_b, 1}^b, \dots, F_{j_b, m_b}^b]\}_{j \in [c]}$, where j_a and j_b are indices such that $ID_{j_a}^a = ID_{j_b}^b = ID_j^{a \cap b}$.
3. Sample two random tables $\langle \mathcal{D} \rangle_a \in \mathbb{Z}_{2^\ell}^{c \times m}$ and $\langle \mathcal{D} \rangle_b \in \mathbb{Z}_{2^\ell}^{c \times m}$ such that $\langle \mathcal{D} \rangle_a + \langle \mathcal{D} \rangle_b = \mathcal{D}$.
4. Return $\langle \mathcal{D} \rangle_a$ to P_a and $\langle \mathcal{D} \rangle_b$ to P_b .

Figure 3: Ideal functionality of Secure Two-Party Data Join.

Security Model. Following prior secure data join schemes [40, 58], in this paper, we consider semi-honest probabilistic polynomial time (PPT) adversaries. A semi-honest PPT adversary \mathcal{A} can corrupt one of the parties P_a or P_b at the beginning of the protocol and aims to learn extra information from the protocol execution while still correctly executing the protocol. We follow the standard simulation-based definition of security for secure two-party computation [10, 47]. We give the formal security definition as follows:

DEFINITION 1 (Semi-honest Model). *Let $\text{view}_C^\Pi(x, y)$ be the views (including input, random tape, and all received messages) of the corrupted party C during the execution of the protocol Π , x be the input of the corrupted party and y be the input of the honest party. Let $\text{out}(x, y)$ be the protocol's output of all parties and $\mathcal{F}(x, y)$ be the functionality's output. Π is said to securely compute a functionality \mathcal{F} in the semi-honest model if for any Probabilistic Polynomial-Time (PPT) adversary \mathcal{A} there exists a simulator Sim_C such that for all inputs x and y ,*

$$\{\text{view}_C^\Pi(x, y), \text{out}(x, y)\} \approx_c \{\text{Sim}_C(x, \mathcal{F}_C(x, y)), \mathcal{F}(x, y)\}.$$

where \approx_c represents computational indistinguishability.

4 DESIGN

Bifrost is instantiated by Protocol 2, which realizes the secure two-party data join functionality $\mathcal{F}_{2PC\text{-}DJoin}$. For simplicity, we assume both parties hold input data with equal row counts (n). **Bifrost** can be directly extended to support parties holding data with different row counts without extra overhead, as detailed in the Appendix A.

Setup, Offline and Online Phase. Similar to prior works [25, 31], operations in **Bifrost** are performed in three distinct phases: (1) offline phase: the two parties perform input-independent precomputations to generate correlated randomness; (2) setup phase: the two parties preprocess their input data, respectively; (3) online phase: the two parties use randomness and the preprocessed data to securely compute the output.

Example: Throughout this section we use a simple example where P_a holds $(ID^a, F^a) = [(aaa, 12), (bbb, 61), (ccc, 37), (ddd, 49)]$, and P_b holds $(ID^b, F^b) = [(ddd, 13), (bbb, 51), (ggg, 28), (eee, 36)]$. In the offline phase, P_a samples two permutations $\pi_1^a : (1 \rightarrow 4, 2 \rightarrow 2, 3 \rightarrow 1, 4 \rightarrow 3)$ and $\pi_2^a : (1 \rightarrow 3, 2 \rightarrow 1, 3 \rightarrow 4, 4 \rightarrow 2)$, and P_b samples two permutations $\pi_1^b : (1 \rightarrow 4, 2 \rightarrow 1, 3 \rightarrow 3, 4 \rightarrow 2)$ and $\pi_2^b : (1 \rightarrow 1, 2 \rightarrow 3, 3 \rightarrow 4, 4 \rightarrow 2)$.

Protocol 2: $\Pi_{2PC-DJoin}$

Parameters: The same as $\mathcal{F}_{2PC-DJoin}$.

Input: P_a inputs its data (ID^a, F^a) . P_b inputs its data (ID^b, F^b) .

Output: P_a and P_b obtain the joined table shares $\langle \mathcal{D} \rangle_a$ and $\langle \mathcal{D} \rangle_b$, respectively.

1. **[Secure Mapped Intersection Generation].** P_a and P_b execute the secure mapped intersection generation protocol Π_{SMIG} (Protocol 3), where P_a inputs its identifiers ID^a , and P_b inputs its identifiers ID^b . After the execution, both parties obtain the mapped intersection index pairs MIPairs.
2. **[Secure Feature Alignment].** P_a and P_b execute the mapped intersection-based secure feature alignment protocol Π_{MI-SFA} (Protocol 4), where P_a inputs its feature columns F^a and mapped intersection pairs MIPairs, and P_b inputs its feature columns F^b and mapped intersection pairs MIPairs. After the execution, P_a and P_b obtain the joined table shares $\langle \mathcal{D} \rangle_a$ and $\langle \mathcal{D} \rangle_b$, respectively.

4.1 Secure Mapped Intersection Generation

In the secure mapped intersection generation step, the two parties execute our proposed secure mapped intersection generation (SMIG) protocol Π_{SMIG} (Protocol 3). Below, we introduce the definition and construction of this protocol.

4.1.1 Definition. As shown in Figure 4, we present a secure mapped intersection generation functionality \mathcal{F}_{SMIG} . \mathcal{F}_{SMIG} takes as input identifiers ID^a from P_a and identifiers ID^b from P_b . It outputs to both parties only the mapped intersection index pairs, denoted by MIPairs. Specifically, $MIPairs = [\pi_1(i), \pi_2(j) \mid (i, j) \in \text{Pairs}_\uparrow]$, where Pairs_\uparrow consists of all intersection index pairs (i, j) with $ID_i^a = ID_j^b$, ordered by i , and π_1, π_2 are permutation (shuffle) functions unknown to both parties. Based on Theorem 1, after the execution of \mathcal{F}_{SMIG} , neither party should learn any extra information beyond what is revealed by the row count c of the joined table.

Functionality \mathcal{F}_{SMIG}

Parameters: The input data row count n .

Input: P_a inputs its identifiers ID^a . P_b inputs its identifiers ID^b .

Functionality:

1. P_a samples two permutations $\pi_1^a, \pi_2^a : [n] \mapsto [n]$. P_b samples two permutations $\pi_1^b, \pi_2^b : [n] \mapsto [n]$. Let $\pi_1 = \pi_1^a \circ \pi_1^b$ and $\pi_2 = \pi_2^b \circ \pi_2^a$.
2. Let $\text{Pairs} = [(i, j) \mid ID_i^a == ID_j^b]$ and let Pairs_\uparrow denote Pairs sorted in ascending order by the first element i of each pair.
3. Define the mapped intersection index pairs $MIPairs = [\pi_1(i), \pi_2(j)]_{(i,j) \in \text{Pairs}_\uparrow}$.
4. Return $MIPairs$ to both P_a and P_b .

Figure 4: Ideal functionality of SMIG.

THEOREM 1. The functionality \mathcal{F}_{SMIG} in Figure 4 reveals no information beyond what is revealed by the joined table row count c to both parties.

PROOF. The proof is presented in Appendix B. \square

4.1.2 Construction. As shown in Protocol 3, the secure mapped intersection generation protocol Π_{SMIG} consists of an offline phase, a setup phase, and an online phase. The online phase of Π_{SMIG} consists of an ECC-based ID encrypting step and a mapped intersection generation step. Below, we introduce these steps in detail.

Offline Phase. Each party P_* ($* \in \{a, b\}$) samples two distinct random permutations $\pi_1^*, \pi_2^* \in [n] \mapsto [n]$. Both parties keep their permutations for future use.

Setup Phase. Each party first locally shuffles its identifiers (IDs) and then encrypts the shuffled IDs using the ECC key. Specifically, (a) For P_a , it first shuffles its IDs with π_1^a to obtain the shuffled IDs $\pi_1^a(ID^a)$. Next, P_a generates an ECC key α and uses α to encrypt the shuffled IDs, obtaining $\alpha H(\pi_1^a(ID^a))$, where $H(\cdot)$ maps each ID to an elliptic-curve point. (b) For P_b , it first shuffles its IDs with π_2^b to obtain the shuffled IDs $\pi_2^b(ID^b)$. Next, P_b generates an ECC key β and uses β to encrypt the shuffled IDs, obtaining $\beta H(\pi_2^b(ID^b))$.

Step 1: ECC-based ID Encrypting. To enable P_a to later obtain the mapped intersection index pairs, the parties engage in an exchange of encrypted IDs using ECC, as follows: (1) P_a sends the encrypted and shuffled IDs $\alpha H(\pi_1^a(ID^a))$ to P_b . (2) P_b first shuffles the received data $\alpha H(\pi_1^a(ID^a))$ with π_1^b to obtain dual-shuffled IDs $\alpha H(\pi_1(ID^a))$, where the composition permutation $\pi_1 = \pi_1^a \circ \pi_1^b$. Next, using its private key β , P_b encrypts the dual-shuffled IDs to obtain the dual-encrypted and dual-shuffled IDs $\beta \alpha H(\pi_1(ID^a)) = [\beta(x)]_{x \in \alpha H(\pi_1(ID^a))}$. Finally, P_b sends $\beta \alpha H(\pi_1(ID^a))$ and its self-shuffled and encrypted IDs $\beta H(\pi_2^b(ID^b))$ to P_a . (3) P_a decrypts the received data $\beta \alpha H(\pi_1(ID^a))$ using its private key α , obtaining $\beta H(\pi_1(ID^a)) = [\alpha^{-1}(x)]_{x \in \beta \alpha H(\pi_1(ID^a))}$. Based on the hardness of the ECDLP, it is computationally infeasible for P_a to recover $H(\pi_1(ID^a))$ from $\beta H(\pi_1(ID^a))$ or recover $H(\pi_2^b(ID^b))$ from $\beta H(\pi_2^b(ID^b))$. At this point, P_a holds $\beta H(\pi_1(ID^a))$ and $\beta H(\pi_2^b(ID^b))$, both encrypted under P_b 's private key β .

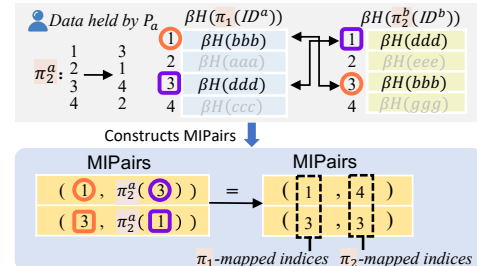


Figure 5: An illustration of constructing MIPairs by P_a in Step 2-(1) of Π_{SMIG} (Protocol 3), using the example data described at the beginning of Section 4.

Step 2: Mapped Intersection Generation. In this step, P_a first obtains the mapped intersection index pairs MIPairs from encrypted data $\beta H(\pi_1(ID^a))$ and $\beta H(\pi_2^b(ID^b))$, both of which are encrypted under P_b 's private ECC key β . We provide a detailed explanation of P_a 's procedure for constructing MIPairs in the next paragraph. Secondly, P_a outputs MIPairs and sends MIPairs to P_b .

P_a 's procedure for constructing MIPairs. As shown in Figure 5, the core idea of this procedure relies on the observation that both $\beta H(\pi_1(ID^a))$ and $\beta H(\pi_2^b(ID^b))$ contain the same encrypted value $\beta H(id)$ for every intersection identifier id . Moreover, $\beta H(\pi_1(ID^a))$ is securely shuffled under the composition permutation π_1 , i.e., $\pi_1^a \circ \pi_1^b$, while $\beta H(\pi_2^b(ID^b))$ is shuffled under P_b 's permutation π_2^b . To generate the mapped intersection index pairs MIPairs, P_a proceeds as follows. For each $i \in [n]$ in $\beta H(\pi_1(ID^a))$, if P_a can find some $j \in [n]$ such that $\beta H(\pi_1(ID^a))_i == \beta H(\pi_2^b(ID^b))_j$,

Protocol 3: Π_{SMIG}

Parameters: The input data row count n . The ECC key bit length σ . A hash function $H(\cdot)$ used for hashing an element to a point on the elliptic curve.

Input: P_a inputs identifiers ID^a . P_b inputs identifiers ID^b .

Output: Both P_a and P_b obtain the mapped intersection index pairs MIPairs.

Offline: P_a samples two random permutations $\pi_1^a, \pi_2^a \in [n] \mapsto [n]$. P_b samples two random permutations $\pi_1^b, \pi_2^b \in [n] \mapsto [n]$.

Setup:

- **[Shuffling and Encrypting Inputs of P_a].** P_a shuffles ID^a with π_1^a to obtain $\pi_1^a(ID^a)$. P_a generates an ECC private key α and computes $\alpha H(\pi_1^a(ID^a)) = [\alpha H(id)]_{id \in \pi_1^a(ID^a)}$.
- **[Shuffling and Encrypting Inputs of P_b].** P_b shuffles ID^b with π_2^b to obtain $\pi_2^b(ID^b)$. P_b generates an ECC private key β and computes $\beta H(\pi_2^b(ID^b)) = [\beta H(id)]_{id \in \pi_2^b(ID^b)}$.

Online:

1. **[ECC-based ID Encrypting].**

- (1) P_a sends $\alpha H(\pi_1^a(ID^a))$ to P_b .
- (2) P_b shuffles $\alpha H(\pi_1^a(ID^a))$ with π_1^b to obtain dual-shuffled IDs $\alpha H(\pi_1^a(ID^a))$, where the composition permutation $\pi_1 = \pi_1^a \circ \pi_1^b$. Then, using its private key β , P_b encrypts the dual-shuffled IDs to obtain the dual-encrypted IDs $\beta \alpha H(\pi_1(ID^a)) = [\beta(x)]_{x \in \alpha H(\pi_1(ID^a))}$. P_b sends this data $\beta \alpha H(\pi_1(ID^a))$ and its encrypted and shuffled IDs $\beta H(\pi_2^b(ID^b))$ to P_a .
- (3) P_a decrypts the received data $\beta \alpha H(\pi_1(ID^a))$ using its private key α , obtaining $\beta H(\pi_1(ID^a)) = [\alpha^{-1}(x)]_{x \in \beta \alpha H(\pi_1(ID^a))}$.

2. **[Mapped Intersection Generation].**

- (1) For $i \in [n]$, if P_a can find some $j \in [n]$ such that $\beta H(\pi_1(ID^a))_i = \beta H(\pi_2^b(ID^b))_j$ (implying both are encrypted from the same intersection identifier id):
 - P_a maps j to $\pi_2^a(j)$. Let i' denote the index of id in ID^b , so that $j = \pi_2^b(i')$ and $\pi_2^a(j) = \pi_2^a(\pi_2^b(i')) = \pi_2(i')$.
 - P_a adds the pair $(i, \pi_2^a(j))$ to MIPairs, where the first and second entries are the π_1 -mapped index of id in ID^a and the π_2 -mapped index of id in ID^b , respectively.
- (2) P_a outputs MIPairs (also sends MIPairs to P_b).

- Index i is exactly the π_1 -mapped index of id in ID^a , since encrypted IDs $\beta H(\pi_1(ID^a))$ is π_1 -shuffled.
- P_a maps j to $\pi_2^a(j)$. Let i' denote the index of id in ID^b , so that $j = \pi_2^b(i')$ and $\pi_2^a(j) = \pi_2^a(\pi_2^b(i')) = \pi_2(i')$, which is the π_2 -mapped index of id in ID^b .
- P_a then appends the pair $(i, \pi_2^a(j))$ to MIPairs, where the first entry is the π_1 -mapped index of id in ID^a and the second entry is the π_2 -mapped index of id in ID^b .

Note that P_a learns no information about the actual values of the intersection IDs, since P_a only obtains encrypted and shuffled IDs.

Example: As shown in Figure 5, after step 1, P_a obtains $\beta H(\pi_1(ID^a))$ and $\beta H(\pi_2^b(ID^b))$. Then, in step 2-(1), P_a constructs the mapped intersection index pairs MIPairs = [(1, 4), (3, 3)], which are then sent to P_b in step 2-(2).

4.2 Secure Feature Alignment

In the secure feature alignment step, based on the outputs of Π_{SMIG} (Protocol 3), P_a and P_b execute our proposed mapped intersection-based secure feature alignment protocol $\Pi_{\text{MI-SFA}}$ to securely obtain the joined table shares $\langle \mathcal{D} \rangle$.

As shown in Protocol 4, $\Pi_{\text{MI-SFA}}$ takes as input feature columns F^a from P_a and feature columns F^b from P_b . In addition, it takes as input the mapped intersection index pairs MIPairs from both parties. After execution, $\Pi_{\text{MI-SFA}}$ outputs to both parties joined table shares $\langle \mathcal{D} \rangle$. $\Pi_{\text{MI-SFA}}$ consists of an offline phase and an online phase. In the offline phase, P_a and P_b generates random matrices required for the online execution of $\Pi_{\text{O-Shuffle}}$ (Protocol 1). The online phase consists of three steps. In steps 1 and 2, P_a and P_b securely dual-shuffle features from P_a and P_b , respectively. For dual-shuffling, each party performs the first-layer shuffle by locally using its permutation and performs the second-layer shuffle by executing $\Pi_{\text{O-Shuffle}}$ (Protocol 1). In step 3, both parties locally extract the shares of the joined table according to the mapped intersection index pairs MIPairs. Below, we introduce these steps in detail.

Offline Phase. Each party P_* ($*$ $\in \{a, b\}$) generates a random matrix $R^* \in \mathbb{Z}_{2^t}^{n \times m^*}$. Using the permutations π_2^b and π_2^a generated in the offline phase of Π_{SMIG} (Protocol 3) by P_b and P_a , respectively, both parties invoke the oblivious shuffle $\mathcal{F}_{\text{O-Shuffle}}$ to obtain the shares of shuffled random matrix, specifically $\langle \pi_2^b(R^a) \rangle, \langle \pi_2^a(R^b) \rangle$.

Step 1: Dual-Shuffling ($\pi_1 = \pi_1^a \circ \pi_1^b$) Features from P_a . Both parties securely obtain shares of P_a 's dual-shuffled features simply as follows: (1) P_a locally shuffles its features F^a with its permutation π_1^a to obtain $\pi_1^a(F^a)$. (2) P_a and P_b jointly execute the online phase of $\Pi_{\text{O-Shuffle}}$ (Protocol 1), where P_a inputs shuffled features $\pi_1^a(F^a)$, random matrix R^a , shuffled random matrix share $\langle \pi_1^b(R^a) \rangle_a$ and receives dual-shuffled feature share $\langle \pi_1^b(\pi_1^a(F^a)) \rangle_a$, i.e., $\langle \pi_1(F^a) \rangle_a$, while P_b inputs its permutation π_1^b (generated in the offline phase of Protocol 3), shuffled random matrix share $\langle \pi_1^b(R^a) \rangle_b$ and receives dual-shuffled feature share $\langle \pi_1(F^a) \rangle_b$. Note that the only communication in the online phase of $\Pi_{\text{O-Shuffle}}$ (Protocol 1) is P_a sending its features masked with random matrix R^a to P_b .

Step 2: Dual-Shuffling ($\pi_2 = \pi_2^b \circ \pi_2^a$) Features from P_b . In a symmetrical step analogous to the first step, the parties now dual-shuffle the features F^b from P_b , with the roles of P_a and P_b exchanged. This process yields dual-shuffled shares $\langle \pi_2(F^b) \rangle_a$ and $\langle \pi_2(F^b) \rangle_b$ to P_a and P_b , respectively.

Step 3: Locally Extract Intersection Data by the Mapped Intersection. This step is straightforward. Each party holds the dual-shuffled feature shares $\langle \pi_1(F^a) \rangle, \langle \pi_2(F^b) \rangle$ and mapped intersection index pairs MIPairs, where each pair are the π_1 -mapped index of intersection identifier id in ID^a and the π_2 -mapped index of intersection identifier id in ID^b . Thus, each party locally extracts shares from $\langle \pi_1(F^a) \rangle$ whose indices are the first entry in each pair of MIPairs and extracts shares from $\langle \pi_2(F^b) \rangle$ whose indices are the second entry in each pair of MIPairs, forming its joined table share. That is, each party collects $\langle \mathcal{D} \rangle = \langle \langle \pi_1(F^a)_i, \pi_2(F^b)_j \rangle \rangle_{(i,j) \in \text{MIPairs}}$.

Example: Recall that the mapped intersection index pairs MIPairs = [(1, 4), (3, 3)] are obtained in Protocol 3. After steps 1 and 2, P_a obtains dual-shuffled feature shares $\langle \pi_1(F^a) \rangle_a = \langle [61, 12, 49, 37] \rangle_a = [43, 8, 23, 9]$ and $\langle \pi_2(F^b) \rangle_a = \langle [36, 28, 13, 51] \rangle_a = [25, 15, 4, 16]$, while P_b obtains dual-shuffled feature shares $\langle \pi_1(F^a) \rangle_b = \langle [61, 12, 49, 37] \rangle_b = [18, 4, 26, 28]$ and $\langle \pi_2(F^b) \rangle_b = \langle [36, 28, 13, 51] \rangle_b = [11, 13, 9, 35]$. In step 3, using MIPairs, each party locally collects $\langle \mathcal{D} \rangle = \langle \langle \pi_1(F^a)_i, \pi_2(F^b)_j \rangle \rangle_{(i,j) \in \text{MIPairs}} = \langle [(61, 51), (49, 13)] \rangle$. That is, P_a obtains the joined table share $\langle \mathcal{D} \rangle_a = [(43, 16), (23, 4)]$, while P_b obtains the joined table share $\langle \mathcal{D} \rangle_b = [(18, 35), (26, 9)]$.

Protocol 4: $\Pi_{\text{MI-SFA}}$

Parameters: The input data row count n . P_a 's feature dimension m_a . P_b 's feature dimension m_b .

Input: P_a inputs feature columns F^a and the mapped intersection index pairs MIPairs. P_b inputs feature columns F^b and the mapped intersection index pairs MIPairs.

Output: P_a and P_b obtain the joined table shares $\langle \mathcal{D} \rangle_a$ and $\langle \mathcal{D} \rangle_b$, respectively, where \mathcal{D} consists of the matched rows.

Offline:

- **[Shuffling Random Matrix of P_a].** P_a samples random matrix $R^a \in \mathbb{Z}_{2^\ell}^{n \times m_a}$. P_a and P_b invoke $\mathcal{F}_{\text{O-Shuffle}}$, where P_a inputs R^a and receives $\langle \pi_1^b(R^a) \rangle_a$, while P_b inputs permutation π_1^b , generated in the offline phase of Π_{SMIG} (Protocol 3), and receives $\langle \pi_1^b(R^a) \rangle_b$.

- **[Shuffling Random Matrix of P_b].** P_b samples random matrix $R^b \in \mathbb{Z}_{2^\ell}^{n \times m_b}$. P_a and P_b invoke $\mathcal{F}_{\text{O-Shuffle}}$, where P_a inputs permutation π_2^a , generated in the offline phase of Π_{SMIG} (Protocol 3), and receives $\langle \pi_2^a(R^b) \rangle_a$, while P_b inputs R^b and receives $\langle \pi_2^a(R^b) \rangle_b$.

Online:

1. **Dual-Shuffling ($\pi_1 = \pi_1^a \circ \pi_1^b$) Features from P_a :**

(1) P_a shuffles its features F^a with π_1^a to obtain $\pi_1^a(F^a)$.
(2) P_a and P_b execute online phase of $\Pi_{\text{O-Shuffle}}$ (Protocol 1), where P_a inputs $\pi_1^a(F^a)$, random matrix R^a , shuffled random matrix share $\langle \pi_1^b(R^a) \rangle_a$ and receives dual-shuffled feature share $\langle \pi_1(F^a) \rangle_a$, while P_b inputs permutation π_1^b , generated in the offline phase of Π_{SMIG} (Protocol 3), shuffled random matrix share $\langle \pi_1^b(R^a) \rangle_b$ and receives dual-shuffled feature share $\langle \pi_1(F^a) \rangle_b$.

2. **Dual-Shuffling ($\pi_2 = \pi_2^b \circ \pi_2^a$) Features from P_b :**

(1) P_b shuffles its features F^b with π_2^b to obtain $\pi_2^b(F^b)$.
(2) P_a and P_b execute online phase of $\Pi_{\text{O-Shuffle}}$ (Protocol 1), where P_b inputs $\pi_2^b(F^b)$, random matrix R^b , shuffled random matrix share $\langle \pi_2^a(R^b) \rangle_b$, and receives dual-shuffled feature share $\langle \pi_2(F^b) \rangle_b$, while P_a inputs permutation π_2^a , generated in the offline phase of Π_{SMIG} (Protocol 3), shuffled random matrix share $\langle \pi_2^a(R^b) \rangle_a$ and receives dual-shuffled feature share $\langle \pi_2(F^b) \rangle_a$.

3. **Locally Extract Intersection Data by the Mapped Intersection Indices:** Each party P_* ($*$ $\in \{a, b\}$) extracts intersection data share from dual-shuffled feature shares according to MIPairs, yielding $\langle \mathcal{D} \rangle_* = \{\langle \pi_1(F^a)_i \rangle_* \| \langle \pi_2(F^b)_j \rangle_*\}_{(i,j) \in \text{MIPairs}}$.

5 SECURITY PROOF

Below, we prove the security of two protocols in Bifrost, namely Π_{SMIG} (Protocol 3) and $\Pi_{\text{MI-SFA}}$ (Protocol 4), against semi-honest adversaries in the two-party setting (the definition of the security model is shown in Section 2).

THEOREM 2. *The SMIG protocol Π_{SMIG} (Protocol 3) securely realizes $\mathcal{F}_{\text{SMIG}}$ in Figure 4 against semi-honest adversary \mathcal{A} .*

PROOF. We exhibit simulators Sim_a and Sim_b for simulating the view of the corrupt P_a and P_b , respectively, and prove that the simulated view is indistinguishable from the real one via standard hybrid arguments.

Case 1 (Corrupt P_a). The simulator Sim_a receives P_a 's input ID^a and P_a 's output MIPairs. Sim_a simulate the view of \mathcal{A} . The incoming messages to \mathcal{A} is encrypted and shuffled IDs $\beta\alpha H(\pi_1(ID^a))$ and $\beta H(\pi_2^b(ID^b))$ received in Online step 1-(2). Sim_a generates the view for \mathcal{A} as follows:

- Sim_a samples an ECC key β from \mathbb{Z}_{2^σ} , two random permutations $\pi_1^b, \pi_2^b : [n] \mapsto [n]$. In addition, Sim_a constructs an n -sized

IDs ID^b by randomly sampling c IDs from P_a 's IDs ID^a and the remaining $n - c$ IDs from the complement of ID^a , where c is the row count of the joined table, i.e., $|\text{MIPairs}|$. Moreover, Sim_a follows the real protocol to sample an ECC key α from \mathbb{Z}_{2^σ} , two random permutations $\pi_1^a, \pi_2^a : [n] \mapsto [n]$.

- Sim_a shuffles ID^a with $\pi_1 = \pi_1^a \circ \pi_1^b$ to obtain $\pi_1(ID^a)$. Sim_a computes $\beta\alpha H(\pi_1(ID^a)) = [\beta\alpha H(id)]_{id \in \pi_1(ID^a)}$.
- Sim_a shuffles ID^b with π_2^b to obtain $\pi_2^b(ID^b)$. Sim_a computes $\beta H(\pi_2^b(ID^b)) = [\beta H(id)]_{id \in \pi_2^b(ID^b)}$.
- Sim_a appends $\beta\alpha H(\pi_1(ID^a))$ and $\beta H(\pi_2^b(ID^b))$ to the view of \mathcal{A} .
- Sim_a follows the real protocol to construct output MIPairs from $\alpha H(\pi_1(ID^a))$ and $\alpha H(\pi_2^b(ID^b))$.
- Sim_a appends MIPairs to the view of \mathcal{A} .

We argue that the view output by Sim_a is indistinguishable from the real one. We first define three hybrid transcripts T_0, T_1, T_2 , where T_0 is the real view of P_a , and T_2 is the output of Sim_a .

1. **Hybrid₀.** The first hybrid is the real interaction described in Protocol 3. Here, an honest party P_b uses real inputs and interacts with the corrupt party P_a . Let T_0 denote the real view of P_a .
2. **Hybrid₁.** Let T_1 be the same as T_0 , except that $\beta\alpha H(\pi_1(ID^a))$ and $\beta H(\pi_2^b(ID^b))$ are replaced by the simulated values. By the security of ECC, the simulated $\beta\alpha H(\pi_1(ID^a))$ and $\beta H(\pi_2^b(ID^b))$ have the same distribution as they would in the real protocol. Hence, T_0 and T_1 are statistically indistinguishable.
3. **Hybrid₂.** Let T_2 be the same as T_1 , except that MIPairs is replaced by the simulated values. For each pair in MIPairs, the first and second entries are exactly the π_1 -mapped index of the intersection identifier id in ID^a and the π_2 -mapped index of the same intersection identifier id in ID^b . In the real view, $\pi_1 = \pi_1^a \circ \pi_1^b$ and $\pi_2 = \pi_2^b \circ \pi_2^a$ are two random composition permutations, which are unknown to P_a , their specific mappings are essentially random. Thus MIPairs are uniformly random over $[n]$. The simulator generates random permutations π_1^b and π_2^b . Even though π_1^a and π_2^a are fixed, applying a uniformly random permutation π_1^b or π_2^b afterward means the final mapping π_1 and π_2 are uniformly random. Thus, the resulting distributions of MIPairs in both the real and simulated views are statistically identical. Therefore, the simulated view is indistinguishable from the real view. This hybrid is exactly the view output by the simulator.

Case 2 (Corrupt P_b). The simulator Sim_b receives P_b 's input ID^b and P_b 's output MIPairs. The incoming view of \mathcal{A} consists of the encrypted and shuffled IDs $\alpha H(\pi_1^a(ID^a))$ received in Online step 1-(1) and the output MIPairs received in Online step 2-(2). Sim_b generates the view for \mathcal{A} as follows:

- Sim_b samples an ECC key α from \mathbb{Z}_{2^σ} , two random permutations $\pi_1^a, \pi_2^a : [n] \mapsto [n]$. In addition, Sim_b constructs an n -sized IDs ID^a by randomly sampling c IDs from P_b 's IDs ID^b and the remaining $n - c$ IDs from the complement of ID^b , where c is the row count of the joined table, i.e., $|\text{MIPairs}|$. Moreover, Sim_b follows the real protocol to sample an ECC key β from \mathbb{Z}_{2^σ} , two random permutations $\pi_1^b, \pi_2^b : [n] \mapsto [n]$.
- Sim_b shuffles ID^a with π_1^a to obtain $\pi_1^a(ID^a)$. Sim_b computes $\alpha H(\pi_1^a(ID^a)) = [\alpha H(id)]_{id \in \pi_1^a(ID^a)}$.
- Sim_b appends $\alpha H(\pi_1^a(ID^a))$ to the view of \mathcal{A} .

- Sim_b computes $\beta H(\pi_1(ID^a))$ and $\beta H(\pi_2^b(ID^b))$. Then, Sim_b involve the procedure for constructing MIPairs.
- Sim_b appends MIPairs to the view of \mathcal{A} .

We argue that the view output by Sim_b is indistinguishable from the real one. We first define three hybrid transcripts T_0, T_1, T_2 , where T_0 is the real view of P_b , and T_2 is the output of Sim_b .

1. *Hybrid*₀. The first hybrid is the real interaction described in Protocol 3. Here, an honest party P_a uses real inputs and interacts with the corrupt party P_b . Let T_0 denote the real view of P_b .
2. *Hybrid*₁. Let T_1 be the same as T_0 , except that $\alpha H(\pi_1^a(ID^a))$ is replaced by the simulated values. By the security of ECC, the simulated $\alpha H(\pi_1^a(ID^a))$ has the same distribution as it would in the real protocol.
3. *Hybrid*₂. Let T_2 be the same as T_1 , except that MIPairs is replaced by the simulated values. Similar to Case 1, in the real view, $\pi_1 = \pi_1^a \circ \pi_1^b$ and $\pi_2 = \pi_2^b \circ \pi_2^a$ are two random permutations, which are unknown to P_a , their specific mappings are essentially random. Thus, MIPairs are uniformly random over $[n]$. The simulator generates random permutations to replace them. Thus, the resulting distributions of MIPairs in both the real and simulated views are statistically identical. This hybrid is exactly the view output by the simulator. \square

THEOREM 3. *The MI-SFA protocol $\Pi_{\text{MI-SFA}}$ (Protocol 4) securely realizes $\mathcal{F}_{\text{MI-SFA}}$ against semi-honest adversary \mathcal{A} .*

PROOF SKETCH. We argue the security of $\Pi_{\text{MI-SFA}}$ by reducing it to the security of its sub-protocol, $\Pi_{\text{O-Shuffle}}$ (Protocol 1). By design, $\Pi_{\text{MI-SFA}}$ involves interaction only during execution of $\Pi_{\text{O-Shuffle}}$. All other steps are performed locally and hence reveal no additional information to the other party. Intuitively, $\Pi_{\text{O-Shuffle}}$ is secure because its only communication step involves sending masked input data $\hat{X} = X - R$, where R is a random matrix with entries sampled uniformly from $\mathbb{Z}_{2^{\ell}}$. This ensures that \hat{X} is uniformly distributed and independent of X , making any two inputs statistically indistinguishable from their masked versions. Consequently, a simulator can output a uniformly random matrix with distribution identical to the real execution. As the security of $\Pi_{\text{O-Shuffle}}$ is formally proven in [40], the security of Protocol 4 follows. \square

6 EVALUATION

Our evaluation aims to answer the following questions:

- Is it beneficial to use the redundancy-free secure data join protocol, **Bifrost**, instead of **CPSI** [52], in the two-step SDA pipeline (secure data join and secure analytics) (Section 6.2)?
- How does **Bifrost** perform relative to the SOTA redundancy-free secure data join protocol, **iPrivJoin** [40] (Section 6.3)?

6.1 Implementation and Experiment Settings

Implementation. We implement **Bifrost** using C++ based on the ECC library `libsodium`². We represent all input data in fixed-point format over the ring $\mathbb{Z}_{2^{64}}$, as in the SDA frameworks [15, 46]. For ECC, we use Curve25519 [7], which provides 128-bit security with a 256-bit key length. The curve equation of Curve25519 is $y^2 = (x^3 + 486662x^2 + x) \bmod (2^{255} - 19)$.

²<https://github.com/jedisct1/libsodium>

Experiment Environment. We perform all experiments on a single Linux server equipped with 2× 10-core 2.4 GHz Intel Xeon Silver 4210R and 1 TB RAM. Each party is simulated by a separate process with one thread. We apply the `tc` tool³ to simulate a WAN setting with a bandwidth of 100 Mbps and 40ms round-trip time, following prior works [30, 40].

Baseline. We consider the following two baselines:

- **iPrivJoin** [40]: To the best of our knowledge, **iPrivJoin** is the only existing protocol that provides the same functionality, i.e., a redundancy-free secure two-party data join protocol, as **Bifrost**. Since **iPrivJoin** is not open-sourced, we re-implemented it, replacing its OPPRF libraries with faster ones [52, 53].
- **CPSI** [52]: **CPSI** [52] is the SOTA circuit-based PSI protocol, which can be used for secure data join. **CPSI** introduces many redundant dummy rows in the joined table (padded to the maximum length), other than the actual matched rows. We reproduce **CPSI**'s results using its open-source code⁴.

For OPPRF, we set the computational security parameter $\kappa = 128$ and the statistical security parameter $\lambda = 40$, consistent with the two baselines. For Cuckoo hashing, we refer to the setting of **CPSI** [52], with $\omega = 1.27$ and 3 hashing functions.

Table 3: Detailed information of datasets.

Dataset	Row Count (n)	Feature Dimension (m)
Education Career Success	5000	19
Breast Cancer Gene	1904	693
Skin Cancer	10000	785
a9a	32561	123
ARCENE	900	10000
MNIST	60000	784
Tiny ImageNet	100000	4096
CelebA	200000	5000

Datasets. Table 3 summarizes all real-world datasets used in our evaluation. To answer the first question (Section 6.2), we use four real-world datasets: Education Career Success [56], Breast Cancer Gene [3], Skin Cancer [63], and a9a [1], to evaluate on secure data join and SDA tasks. To answer the second question (Section 6.3), we first evaluate **Bifrost** on eight datasets: the above four plus ARCENE [23], MNIST [37], Tiny ImageNet [36], and the large-scale CelebA [41], following prior SDA studies [46, 61]. These datasets vary in row counts (from 900 to 200000) and feature dimensions (from 19 to 10000). For each dataset, we perform vertical partitioning, where the two parties hold disjoint feature columns but share the same row count as the original dataset. We set the intersection rate to $\rho = 80\%$, consistent with **iPrivJoin** [40]. Specifically, we randomly select 80% overlapping samples and fill the remaining 20% of non-overlapping rows with randomly generated samples. As analyzed in Appendix C, the intersection rate (ρ) has a negligible impact on the performance of the baselines and **Bifrost**, so setting $\rho = 80\%$ provides a fair comparison. In addition, we configure that P_a holds the data with a greater number of feature columns, as the baselines are more efficient in this setup compared to the reverse configuration (see Section 6.3.3 for details). Furthermore, we generate synthetic datasets with sizes up to 100 GB to evaluate efficiency under varying parameters.

³<https://man7.org/linux/man-pages/man8/tc.8.html>

⁴<https://github.com/Visa-Research/volepsi.git>

Table 4: End-to-end online comparison of Bifrost, iPrivJoin [40] and CPSI [52] on two types of SDA tasks: secure statistical analysis and secure training (the term "secure" is omitted in the table). The costs of the SDA tasks for Bifrost and iPrivJoin are identical, as both produce the same inputs for SDA tasks. The efficiency of secure training is evaluated in one epoch.

Steps	Education Career Success						Breast Cancer Gene						
	Time (s)			Communication (MB)			Time (s)			Communication (MB)			
	Bifrost	iPrivJoin [40]	CPSI [52]	Bifrost	iPrivJoin [40]	CPSI [52]	Bifrost	iPrivJoin [40]	CPSI [52]	Bifrost	iPrivJoin [40]	CPSI [52]	
Secure Data Join	1.17	2.94	3.61	1.21	7.96	7.36	1.46	19.37	11.83	10.25	67.44	61.53	
Statistical Analyze		3.04		8.50		0.50	1.86		11.19	21.50		103.22	186.63
Total	4.21	5.98	12.11	1.71	8.46	9.22	12.65	30.56	33.33	113.47	170.66	248.16	

Steps	Skin Cancer						a9a						
	Time (s)			Communication (MB)			Time (s)			Communication (MB)			
	Bifrost	iPrivJoin [40]	CPSI [52]	Bifrost	iPrivJoin [40]	CPSI [52]	Bifrost	iPrivJoin [40]	CPSI [52]	Bifrost	iPrivJoin [40]	CPSI [52]	
Secure Data Join	7.11	108.07	73.63	60.87	385.51	319.05	8.24	61.88	33.62	33.98	247.85	228.79	
Training		2371.44		3735.75		683.14	1073.44		7181.97	11365.90		290.28	459.31
Total	2378.55	2479.51	3809.38	744.01	1068.65	1392.49	7190.21	7243.85	11399.52	324.26	538.13	688.10	

6.2 Two-step SDA Pipeline Evaluation

We compare CPSI [52], iPrivJoin [40], and Bifrost in a two-step SDA pipeline: secure data join and SDA task execution. The SDA task leverages the outputs of secure data join as its input data.

SDA tasks. We evaluate two types of SDA tasks: secure statistical analysis and secure training. (1) For secure statistical analysis, we examine the following two scenarios:

- Chi-square test: an education department and a tax department securely compute a chi-square test value on education data and income data [16]. To simulate this scenario, the feature columns in the Education Career Success dataset [56] are vertically partitioned into education-related and income-related features, which are held separately by the two parties.
- Pearson correlation: a hospital and a genomic company securely compute the Pearson correlation between disease and gene data [39]. To simulate this scenario, the feature columns in the Breast Cancer Gene dataset [3] are vertically partitioned into disease-related features and gene-related features, which are held separately by the two parties.

We design secure Chi-square test and secure Pearson correlation protocols (provided in Appendix D). Both are implemented using SMPC primitives in MP-SPDZ [30]. (2) For secure training, we examine two scenarios: One party holds users' image data while the other holds their labels; two parties hold disjoint subsets of users' features. In both scenarios, the parties aim to securely train a model on the joined table shares. We use the Skin Cancer [63] and a9a [1] datasets to simulate the above two scenarios, respectively. We employ MP-SPDZ [30], a widely used open-source SMPC framework, to securely train logistic regression models over 10 epochs.

In terms of efficiency, Table 4 shows that Bifrost significantly accelerates the secure data join process, achieving up to $10.36\times$ faster running time and up to $6.73\times$ reduction in communication size compared to CPSI, and up to $15.20\times$ faster running time and up to $7.29\times$ reduction in communication size compared to iPrivJoin. The inferior performance of iPrivJoin relative to CPSI stems from its reliance on multiple rounds of oblivious shuffling to remove redundant rows present in CPSI. An important observation is that, during the downstream SDA process, CPSI incurs an increase of $1.58 \sim 2.80\times$ in running time and $1.57 \sim 3.72\times$ in communication size. The inefficiency of the SDA process caused by CPSI arises from the redundant padded outputs in the join results. Specifically, CPSI

outputs a joined table of row count $N = \omega \cdot n$ (with $\omega = 1.27$ in our experiments), where $\rho \cdot n$ rows are intersection data (intersection rate ρ). For $\rho = 80\%$, the redundant fraction of CPSI's outputs is $((\omega - \rho) \cdot n) / N \approx 37.01\%$. In terms of correctness, Table 5 shows that CPSI leads to catastrophic error rate blowup in downstream secure statistical analysis and degrades the accuracy of secure training, with the Chi-square test statistic deviating by up to 13858.55%. Due to the limited performance and accuracy of CPSI, we exclude it from subsequent secure data join evaluations.

Table 5: Correctness of SDA tasks: Bifrost vs. CPSI [52] compared to performing data analytics on plaintext. ('Education' = Education Career Success, 'Breast' = Breast Cancer Gene).

SDA tasks Dataset	Stats. Percent Error		Training Accuracy Bias	
	Education	Breast	Skin Cancer	a9a
Bifrost	0.00%	0.08%	-0.27%	-0.42%
CPSI [52]	13858.55%	77.20%	-0.36%	-0.50%

6.3 Secure Data Join Evaluation

6.3.1 Evaluation on Real-World Datasets across Three Phases. We compare Bifrost with iPrivJoin [40] across three phases (offline, setup, and online) using eight real-world datasets summarized in Table 3. Detailed results are provided in Appendix E.1. Table 6 and Figure 6 highlight the key results, summarized as follows:

- In the online phase, Bifrost significantly outperforms iPrivJoin by $2.54 \sim 19.64\times$ in running time. Moreover, Bifrost outperforms iPrivJoin by $1.40 \sim 3.75\times$ in memory cost. The performance gain of Bifrost mainly stems from a reduction of $84.15\% \sim 86.29\%$ in communication size compared to iPrivJoin. Specifically, the inefficiency of iPrivJoin stems from using cryptographic primitive OPPRF and multiple rounds of oblivious shuffle for redundant data removal. In contrast, Bifrost requires a single round of oblivious shuffle while eliminating OPPRF. In addition, Bifrost requires only 4 communication rounds, fewer than the 11 rounds required by iPrivJoin.
- Considering both the setup and online phases, Bifrost achieves an average speedup of $17.59\times$ over iPrivJoin. Despite incurring high computational overhead in the setup phase due to ECC operations, Bifrost maintains superior overall performance. In addition, considering all three phases, Bifrost achieves an

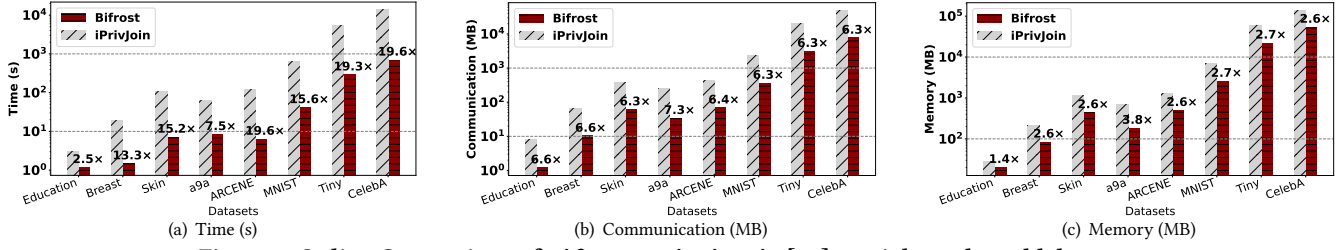


Figure 6: Online Comparison of Bifrost vs. iPrivJoin [40] on eight real-world datasets.

average speedup of $2.57\times$ in running time and a $2.59\times$ reduction in communication size. This improvement is primarily attributed to Bifrost’s offline phase, which requires less than half of the communication size of iPrivJoin.

- The performance advantage of Bifrost scales with dataset size: on the largest dataset, CelebA (15 GB), iPrivJoin requires 227.20 minutes to complete the join, whereas Bifrost finishes in only 11.57 minutes, yielding a $19.64\times$ speedup in online running time, thereby highlighting its superior efficiency and scalability.

Table 6: Average comparison of Bifrost vs. iPrivJoin [40] across three phases on eight real-world datasets.

Protocol	Offline		Setup		Online	
	Time (s)	Comm. (MB)	Time (s)	Time (s)	Comm. (MB)	
Bifrost	11754.62 (2.39 \times)	88307.52 (2.53 \times)		12.28	130.86 (19.24 \times)	1415.78 (6.34 \times)
iPrivJoin [40]	28059.99	223704.32		0.22	2518.01	8983.04

In the following evaluation across varying parameters, we focus exclusively on the online-phase performance using datasets up to 100 GB. Results on smaller-scale datasets are given in Appendix E.2, and offline-phase performance results are given in Appendix E.3.

6.3.2 *Evaluation across Different Row Counts.* We conduct experiments on datasets of row count n from 2^{14} to 2^{20} with a fixed feature dimension ($m_a = m_b = 6400$), which corresponds to dataset sizes scaling from 1.56 GB up to 100 GB. As shown in Figure 7, Bifrost significantly outperforms iPrivJoin by $21.40 \sim 15.85\times$ in running time and $7.70 \sim 7.73\times$ in communication size. Furthermore, the runtime advantage of Bifrost remains steady at $21.59\times$, and its communication size reduction remains at about 7.73%. This is because both Bifrost and iPrivJoin have communication and computation costs that grow linearly in n . Therefore, the relative efficiency advantage remains stable for fixed feature dimensions.

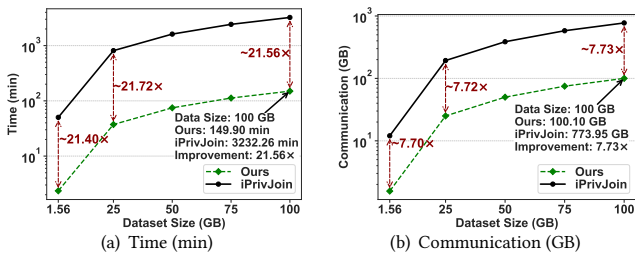


Figure 7: Comparison of Bifrost vs. iPrivJoin [40] on varying row counts when fixing feature dimension.

6.3.3 *Evaluation across Different Feature Dimensions.* We evaluate the effect of feature dimensionality under two settings: (1) We vary the feature dimensions $m_a = m_b$ from 100 to 6400 while fixing the dataset size at $n = 2^{20}$. (2) We vary one party’s feature dimension m_* from 100 to 6400, where $* \in \{a, b\}$, while fixing the other party’s feature dimension to 100 and the dataset size to $n = 2^{20}$. The corresponding results are presented in Figure 8(a) and Figure 8(b), respectively. We summarize as follows:

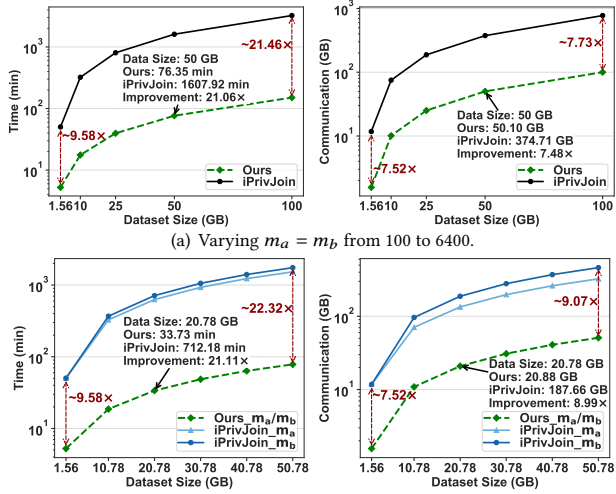
- Bifrost outperforms iPrivJoin by $9.58 \sim 22.32\times$ in running time and $7.52 \sim 9.07\times$ in communication size. In addition, the performance improvement of Bifrost becomes more pronounced as the feature dimension increases. For instance, as $m_a = m_b$ increases from 100 to 6400, the running time improvement of Bifrost over iPrivJoin increases from $9.58\times$ to $21.46\times$. This trend occurs because the computational and communication costs of iPrivJoin grow more rapidly with the feature dimension than those of Bifrost. Therefore, Bifrost exhibits better efficiency when the feature dimension is large.
- Bifrost achieves better performance compared to iPrivJoin, up to $22.32\times$ when increasing only m_b and up to $19.52\times$ when increasing only m_a . The gap widens as m_b grows because iPrivJoin must share P_b ’s features with P_a via OPPRF, whereas Bifrost avoids this bottleneck. Thus Bifrost scales more efficiently when one party holds higher-dimensional features.

6.3.4 *Unbalanced Setting Experiments.* One special scenario is the unbalanced setting [25, 58], where the row count of the two parties’ datasets differs by at least two orders of magnitude. We conduct experiments with the SOTA secure unbalanced and redundancy-free data join protocol Suda [58]. The results demonstrate that Bifrost achieves $4.78 \sim 5.04\times$ faster running time compared to Suda in unbalanced settings (see Appendix E.4).

7 DISCUSSION

Supporting Join on Non-Key Attributes. For non-key attributes, there are two cases. In the first case, the attribute is unique within each table. The parties can treat this attribute as the identifiers and directly apply Bifrost to perform secure joins. In the second case, the attribute is non-unique, which means multiple records may share the same attribute value. Handling non-unique attributes requires additional steps beyond the scope of this work, and we leave this as future work.

Strengthening the Threat Model. Bifrost, which is secure under the semi-honest model, can be strengthened to provide security under a stronger threat model that accounts for specific malicious protocol deviations. We outline the strengthening path of Bifrost



(b) Varying m_a (m_b) from 100 to 6400 when fixing m_b (m_a). $iPrivJoin_{m_a}$ and $iPrivJoin_{m_b}$ denote the performance of $iPrivJoin$ when varying m_a and m_b , respectively; $Ours_{m_a/m_b}$ denotes the performance of Bifrost under either variation and is plotted as a single curve because m_a and m_b affect Bifrost identically.

Figure 8: Comparison of Bifrost vs. $iPrivJoin$ [40] on varying feature dimensions when fixing row count.

(comprising Π_{SMIG} and Π_{MI-SFA}) toward this stronger threat model as follows: (i) For Π_{SMIG} (Protocol 3), we can integrate a commitment scheme and Non-Interactive Zero-Knowledge proofs (NIZKs) to ensure that ECC-based ID encrypting is executed correctly, preventing malicious parties from using invalid keys; (ii) For Π_{MI-SFA} (Protocol 4), we can replace its underlying semi-honest oblivious shuffle protocol ($\Pi_{O-Shuffle}$) with a malicious-secure shuffle protocol [59] to ensure that each party correctly shuffles the other party’s features. See Appendix F for a detailed discussion.

8 RELATED WORK

Circuit-based PSI. The initial CPSI protocol is introduced by Huang *et al.* [28], which allows two parties, each with input X and Y , to output the secret-shared $X \cap Y$ without revealing any other information. Since the outputs are secret-shared, they can be directly used in subsequent MPC protocols, such as secure model training. In this way, CPSI can be employed to perform secure data join. Subsequent research on CPSI primarily follows two directions: those based on OPPRF [11, 21, 34, 50, 52, 53] and others based on private set membership [14, 42]. A number of works [25, 43, 57] also focus on designing efficient CPSI protocols for unbalanced settings. Despite these innovations, CPSI inherently introduces many redundant dummy rows (i.e., secret-shared zeros) in the joined table (padded to the maximum length), other than the actual matched rows. These redundant rows result in significant overhead to downstream secure data analytics tasks in many practical scenarios.

Balanced Secure Data Join Scheme. To address the above limitation in CPSI, Liu *et al.* propose $iPrivJoin$ [40]. To remove the redundant rows, $iPrivJoin$ introduces excessive communication overhead in the secure data join process, which stems from its reliance on OPPRF [53] and multiple rounds of oblivious shuffle.

Unbalanced Secure Data Join Scheme. Real-world scenarios may involve unbalanced datasets [58], where one party’s dataset row

count is significantly smaller than the other’s. Song *et al.* propose the SOTA secure *unbalanced* data join framework Suda [58]. They leverage polynomial-based operations to efficiently output (the secret shares of) the redundancy-free joined table. However, it scales inefficiently when directly applied to balanced settings, which are common and foundational settings.

Others. (1) Secure data join schemes [20, 26, 55] for vertical federated learning rely on a Trusted Third Party (TTP), which may impose a strong trust assumption in practical scenarios. (2) Private Set Union (PSU) scheme [60, 67] enables secure data join without a TTP but pads non-overlapping parts with synthetic data, resulting in redundant outputs. (3) Enclave-based scheme [17, 35, 69] executes joins inside trusted hardware execution environments, which can reduce cryptographic overheads but inherit enclave trust.

We summarize representative secure data join schemes in Table 7.

Table 7: High-level comparison of various secure data join schemes with simplified communication complexity. Here, n is the row count of the input data; m_a and m_b are the feature dimensions for P_a and P_b , respectively; $m = m_a + m_b$; ℓ and ℓ' are the bit-lengths of the element and the encrypted element, respectively; λ and κ are the statistical security parameter and the computational security parameter, respectively.

Scheme	Communication complexity	Limitation
Ours	$O(nml)$	–
$iPrivJoin$ [40]	$O(nm_b\kappa + nml)$	High communication overhead
CPSI [52]	$O(nm_b\kappa + nml)$	Redundant rows
Suda [58]	$O(nml)$	Designed for unbalanced setting
FL-Join [26]	$O(nml')$	Relies on a trusted third party
PSU [67]	$O((n + n \log n)m\ell)$	Redundant synthetic rows
Enclave-Join [35]	–	Relies on enclave trust

9 CONCLUSION

In this paper, we propose an efficient and simple secure two-party data join protocol, referred to as Bifrost. Bifrost outputs (the secret shares of) the redundancy-free joined table. The highlight of Bifrost lies in its simplicity: Bifrost builds upon two conceptually simple building blocks, an ECDH-PSI protocol and an oblivious shuffle protocol. The lightweight protocol design allows Bifrost to avoid many performance bottlenecks in the SOTA redundancy-free secure two-party data join protocol, $iPrivJoin$, including the need for Cuckoo hashing and OPPRF. We also propose an optimization named *dual mapping* that reduces the rounds of oblivious shuffle needed from two to one. Compared to the SOTA redundancy-free protocol $iPrivJoin$ [40], Bifrost achieves $4.41 \sim 12.96 \times$ faster running time and reduces communication size by $64.32\% \sim 80.07\%$. Moreover, experiments on two-step SDA (secure join and secure analytics) show that Bifrost’s redundancy-free design avoids error blowup caused by redundant padded outputs (unlike CPSI), while delivering up to $2.80 \times$ faster secure analytics with up to 73.15% communication reduction compared to CPSI.

ACKNOWLEDGMENTS

This work was supported by the National Cryptologic Science Fund of China (Number 2025NCSF01010) and the Natural Science Foundation of China (Number 92370120).

REFERENCES

[1] 2001. a9a dataset. LIBSVM datasets. <https://www.csie.ntu.edu.tw/~cjlin/libsvmtools/datasets/binary.html>

[2] Rakesh Agrawal and Ramakrishnan Srikant. 2000. Privacy-preserving data mining. In *Proceedings of the 2000 ACM SIGMOD international conference on Management of data*. 439–450.

[3] Raghad Alharbi. 2022. Breast Cancer Gene Expression Profiles (METABRIC). <https://www.kaggle.com/datasets/raghadalharbi/breast-cancer-gene-expression-profiles-metabric/data>

[4] Demetrios Avraam, Rebecca Wilson, Oliver Butters, Thomas Burton, Christos Nicolaides, Elinor Jones, Andy Boyd, and Paul Burton. 2021. Privacy preserving data visualizations. *EPJ Data Science* 10 (01 2021). <https://doi.org/10.1140/epjds/s13688-020-00257-4>

[5] Ahmad Taher Azar and Shereen M El-Metwally. 2013. Decision tree classifiers for automated medical diagnosis. *Neural Computing and Applications* 23 (2013), 2387–2403.

[6] Joes Bater, Gregory Elliott, Craig Eggen, Satyender Goel, Abel Kho, and Jennie Rogers. 2016. SMQCL: secure querying for federated databases. *arXiv preprint arXiv:1606.06808* (2016).

[7] Daniel J Bernstein. 2006. Curve25519: new Diffie-Hellman speed records. In *Public Key Cryptography-PKC 2006: 9th International Conference on Theory and Practice in Public-Key Cryptography*, New York, NY, USA, April 24–26, 2006. *Proceedings* 9. Springer, 207–228.

[8] R. Bonta. 2022. California Consumer Privacy Act (CCPA). <https://oag.ca.gov/privacy/ccpa> Retrieved from State of California Department of Justice.

[9] Nicolas Bruno, YongChul Kwon, and Ming-Chuan Wu. 2014. Advanced join strategies for large-scale distributed computation. *Proc. VLDB Endow.* 7, 13 (Aug. 2014), 1484–1495. <https://doi.org/10.14778/2733004.2733020>

[10] Ran Canetti. 2001. Universally composable security: A new paradigm for cryptographic protocols. In *Proceedings 42nd IEEE Symposium on Foundations of Computer Science*. IEEE, 136–145.

[11] Nishanth Chandran, Divya Gupta, and Akash Shah. 2021. Circuit-PSI with linear complexity via relaxed batch OPPRF. *Cryptography ePrint Archive* (2021).

[12] Tianyi Chen, Xiao Jin, Yuejiao Sun, and Wotao Yin. 2020. Vafl: a method of vertical asynchronous federated learning. *arXiv preprint arXiv:2007.06081* (2020).

[13] Kewei Cheng, Tao Fan, Yilun Jin, Yang Liu, Tianjian Chen, Dimitrios Papadopoulos, and Qiang Yang. 2021. SecureBoost: A Lossless Federated Learning Framework. *IEEE Intelligent Systems* 36, 06 (Nov. 2021), 87–98. <https://doi.org/10.1109/MIS.2021.3082561>

[14] Michele Ciampi and Claudio Orlandi. 2018. Combining private set-intersection with secure two-party computation. In *International Conference on Security and Cryptography for Networks*. Springer, 464–482.

[15] Daniel Demmler, Thomas Schneider, and Michael Zohner. 2015. ABY-A framework for efficient mixed-protocol secure two-party computation. In *22nd Annual Network and Distributed System Security Symposium (NDSS)*.

[16] George Drosatos and Pavlos S Efraimidis. 2011. Privacy-preserving statistical analysis on ubiquitous health data. In *International conference on trust, privacy and security in digital business*. Springer, 24–36.

[17] Saba Eskandarian and Matei Zaharia. 2019. OblivDB: oblivious query processing for secure databases. *Proc. VLDB Endow.* 13, 2 (Oct. 2019), 169–183. <https://doi.org/10.14778/3364324.3364331>

[18] David Evans, Vladimir Kolesnikov, Mike Rosulek, et al. 2018. A pragmatic introduction to secure multi-party computation. *Foundations and Trends® in Privacy and Security* 2, 2–3 (2018), 70–246.

[19] Amos Fiat and Adi Shamir. 1986. How to prove yourself: Practical solutions to identification and signature problems. In *Conference on the theory and application of cryptographic techniques*. Springer, 186–194.

[20] Ying Gao, Yuxin Xie, Huanghao Deng, Zukun Zhu, and Yiyu Zhang. 2024. A Privacy-preserving Data Alignment Framework for Vertical Federated Learning. *Journal of Electronics & Information Technology* 46, 8 (2024), 3419–3427. <https://doi.org/10.11999/JEIT231234>

[21] Gayathri Garimella, Benny Pinkas, Mike Rosulek, Ni Trieu, and Avishay Yanai. 2021. Oblivious key-value stores and amplification for private set intersection. In *Advances in Cryptology-CRYPTO 2021: 41st Annual International Cryptology Conference, CRYPTO 2021, Virtual Event, August 16–20, 2021, Proceedings, Part II* 41. Springer, 395–425.

[22] Jens Groth. 2016. On the size of pairing-based non-interactive arguments. In *Annual international conference on the theory and applications of cryptographic techniques*. Springer, 305–326.

[23] Guyon, I. and Gunn, S. and Ben-Hur, A. and Dror, G. 2004. Arcene Dataset. UCI Machine Learning Repository. <https://doi.org/10.24432/C58P55> Accessed: 2016-07-14.

[24] Darrel Hankerson, Alfred J Menezes, and Scott Vanstone. 2004. *Guide to elliptic curve cryptography*. Springer Science & Business Media.

[25] Meng Hao, Weiran Liu, Liqiang Peng, Hongwei Li, Cong Zhang, Hanxiao Chen, and Tianwei Zhang. 2024. Unbalanced Circuit-PSI from Oblivious Key-Value Retrieval. In *33rd USENIX Security Symposium (USENIX Security 24)*. 6435–6451.

[26] Stephen Hardy, Wilko Henecka, Hamish Ivey-Law, Richard Nock, Giorgio Patrini, Guillaume Smith, and Brian Thorne. 2017. Private federated learning on vertically partitioned data via entity resolution and additively homomorphic encryption. *arXiv preprint arXiv:1711.10677* (2017).

[27] Daojing He, Rummeng Du, Shanshan Zhu, Min Zhang, Kaitai Liang, and Sammy Chan. 2022. Secure Logistic Regression for Vertical Federated Learning. *IEEE Internet Computing* 26, 2 (2022), 61–68. <https://doi.org/10.1109/MIC.2021.3138853>

[28] Yan Huang, David Evans, and Jonathan Katz. 2012. Private set intersection: Are garbled circuits better than custom protocols?. In *19th Annual Network and Distributed System Security Symposium (NDSS)*.

[29] Bernardo A Huberman, Matt Franklin, and Tad Hogg. 1999. Enhancing privacy and trust in electronic communities. In *Proceedings of the 1st ACM conference on Electronic commerce*. 78–86.

[30] Marcel Keller. 2020. MP-SPDZ: A Versatile Framework for Multi-Party Computation. In *Proceedings of the 2020 ACM SIGSAC Conference on Computer and Communications Security*. <https://doi.org/10.1145/3372297.3417872>

[31] Florian Kerschbaum, Erik-Oliver Blass, and Rasoul Akhavan Mahdavi. 2023. Faster Secure Comparisons with Offline Phase for Efficient Private Set Intersection. In *30th Annual Network and Distributed System Security Symposium (NDSS)*. The Internet Society, San Diego, California, USA. <https://doi.org/10.14722/ndss.2023.23198>

[32] Bas Ketsman and Dan Suciu. 2017. A Worst-Case Optimal Multi-Round Algorithm for Parallel Computation of Conjunctive Queries. In *Proceedings of the 36th ACM SIGMOD-SIGACT-SIGAI Symposium on Principles of Database Systems (Chicago, Illinois, USA) (PODS '17)*. Association for Computing Machinery, New York, NY, USA, 417–428. <https://doi.org/10.1145/3034786.3034788>

[33] Neal Koblitz. 1987. Elliptic curve cryptosystems. *Mathematics of computation* 48, 177 (1987), 203–209.

[34] Vladimir Kolesnikov, Naor Matanai, Benny Pinkas, Mike Rosulek, and Ni Trieu. 2017. Practical multi-party private set intersection from symmetric-key techniques. In *Proceedings of the 2017 ACM SIGSAC Conference on Computer and Communications Security*. 1257–1272.

[35] Simeon Krastnikov, Florian Kerschbaum, and Douglas Stebila. 2020. Efficient oblivious database joins. *Proc. VLDB Endow.* 13, 12 (July 2020), 2132–2145. <https://doi.org/10.14778/3407790.3407814>

[36] Yann Le and Xuan Yang. 2015. Tiny imagenet visual recognition challenge. *CS* 231N 7, 7 (2015), 3.

[37] LeCun, Yann and Cortes, Corinna and Burges, Christopher J.C. 2010. MNIST handwritten digit database. <http://yann.lecun.com/exdb/mnist/> Accessed: 2016-07-14.

[38] Guopeng Lin, Ruisheng Zhou, Shuyu Chen, Weili Han, Jin Tan, Wenjing Fang, Lei Wang, and Tao Wei. 2025. Kona: An Efficient Privacy-Preservation Framework for KNN Classification by Communication Optimization. In *Forty-second International Conference on Machine Learning*. <https://openreview.net/forum?id=1VqxlgyQlp>

[39] Yehuda Lindell. 2020. Secure multiparty computation. *Commun. ACM* 64, 1 (2020), 86–96.

[40] Yang Liu, Bingsheng Zhang, Yuxiang Ma, Zhuo Ma, and Zecheng Wu. 2023. iPrivJoin: An ID-Private Data Join Framework for Privacy-Preserving Machine Learning. *IEEE Transactions on Information Forensics and Security* (2023).

[41] Ziwei Liu, Ping Luo, Xiaogang Wang, and Xiaou Tang. 2015. Deep Learning Face Attributes in the Wild. In *Proceedings of International Conference on Computer Vision (ICCV)*.

[42] Jack PK Ma and Sherman SM Chow. 2022. Secure-computation-friendly private set intersection from oblivious compact graph evaluation. In *Proceedings of the 2022 ACM on Asia Conference on Computer and Communications Security*. 1086–1097.

[43] Rasoul Akhavan Mahdavi, Nils Lukas, Faezeh Ebrahimiaghazani, Thomas Humphries, Bailey Kacsmar, John Premkumar, Xinda Li, Simon Oya, Ehsan Amjadian, and Florian Kerschbaum. 2024. PEPSI: Practically Efficient Private Set Intersection in the Unbalanced Setting. In *33rd USENIX Security Symposium (USENIX Security 24)*. 6453–6470.

[44] Catherine Meadows. 1986. A more efficient cryptographic matchmaking protocol for use in the absence of a continuously available third party. In *1986 IEEE Symposium on Security and Privacy*. IEEE, 134–134.

[45] Victor S Miller. 1985. Use of elliptic curves in cryptography. In *Conference on the theory and application of cryptographic techniques*. Springer, 417–426.

[46] Payman Mohassel and Yupeng Zhang. 2017. Secureml: A system for scalable privacy-preserving machine learning. In *2017 IEEE symposium on security and privacy (SP)*. IEEE, 19–38.

[47] Goldreich Oded. 2009. Foundations of cryptography: Volume 2, basic applications.

[48] Anifat Olawoyin, Carson Leung, and Alfredo Cuzzocrea. 2021. Privacy-Preserving Publishing and Visualization of Spatial-Temporal Information. In *2021 IEEE International Conference on Big Data (Big Data)*. IEEE, 5420–5429.

https://doi.org/10.1109/BigData52589.2021.9671564

[49] Torben Pryds Pedersen. 1991. Non-interactive and information-theoretic secure verifiable secret sharing. In *Annual international cryptology conference*. Springer, 129–140.

[50] Benny Pinkas, Thomas Schneider, Oleksandr Tkachenko, and Avishay Yanai. 2019. Efficient circuit-based PSI with linear communication. In *Advances in Cryptology–EUROCRYPT 2019: 38th Annual International Conference on the Theory and Applications of Cryptographic Techniques, Darmstadt, Germany, May 19–23, 2019, Proceedings, Part III* 38. Springer, 122–153.

[51] Rishabh Poddar, Sukrit Kalra, Avishay Yanai, Ryan Deng, Raluca Ada Popa, and Joseph M Hellerstein. 2021. Senate: a Maliciously-Secure MPC platform for collaborative analytics. In *30th USENIX Security Symposium (USENIX Security 21)*. 2129–2146.

[52] Peter Rindal and Srinivasan Raghuraman. 2022. Blazing Fast PSI from Improved OKVs and Subfield VOLE. *IACR Cryptol. ePrint Arch.* 2022 (2022), 320.

[53] Peter Rindal and Philipp Schoppmann. 2021. VOLE-PSI: fast OPRF and circuit-PSI from vector-ole. In *Advances in Cryptology–EUROCRYPT 2021: 40th Annual International Conference on the Theory and Applications of Cryptographic Techniques, Zagreb, Croatia, October 17–21, 2021, Proceedings, Part II*. Springer, 901–930.

[54] Wolf Rödiger, Sam Idicula, Alfons Kemper, and Thomas Neumann. 2016. Flow-Join: Adaptive Skew Handling for Distributed Joins Over High-Speed Networks. In *Proceedings of the 32nd IEEE International Conference on Data Engineering (ICDE ’16)*. IEEE Computer Society, Los Alamitos, CA, USA, 1194–1205. <https://doi.org/10.1109/ICDE.2016.7498324>

[55] Rainer Schnell, Tobias Bachteler, and Jörg Reiher. 2011. A novel error-tolerant anonymous linking code. *Available at SSRN 3549247* (2011).

[56] Adil Shamim. 2024. Education and Career Success. <https://www.kaggle.com/datasets/adilshamim8/education-and-career-success/data>

[57] Yongha Son and Jinkyung Jeong. 2023. PSI with computation or Circuit-PSI for Unbalanced Sets from Homomorphic Encryption. In *Proceedings of the 2023 ACM Asia Conference on Computer and Communications Security*. 342–356.

[58] Lushan Song, Qizhi Zhang, Yu Lin, Haoyu Niu, Daode Zhang, Zheng Qu, Weili Han, Jue Hong, Quanwei Cai, and Ye Wu. 2025. Suda: An Efficient and Secure Unbalanced Data Alignment Framework for Vertical Privacy-Preserving Machine Learning. In *34th USENIX Security Symposium (USENIX Security 25)*. 7663–7682.

[59] Xiangfu Song, Dong Yin, Jianli Bai, Changyu Dong, and Ee-Chien Chang. 2024. Secret-Shared Shuffle with Malicious Security. In *31st Annual Network and Distributed System Security Symposium (NDSS)*. <https://doi.org/10.14722/ndss.2024.24021>

[60] Jiankai Sun, Xin Yang, Yuanshun Yao, Aonan Zhang, Weihao Gao, Junyuan Xie, and Chong Wang. 2021. Vertical federated learning without revealing intersection membership. *arXiv preprint arXiv:2106.05508* (2021).

[61] Sijun Tan, Brian Knott, Yuan Tian, and David J Wu. 2021. CryptGPU: Fast privacy-preserving machine learning on the GPU. In *2021 IEEE Symposium on Security and Privacy (SP)*. IEEE, 1021–1038.

[62] Yongxin Tong, Xuchen Pan, Yuxiang Zeng, Yexuan Shi, Chunbo Xue, Zimu Zhou, Xiaofei Zhang, Lei Chen, Yi Xu, Ke Xu, et al. 2022. Hu-fu: Efficient and secure spatial queries over data federation. *Proceedings of the VLDB Endowment* 15, 6 (2022), 1159.

[63] Philipp Tscharndl, Cliff Rosendahl, and Harald Kittler. 2018. The HAM10000 dataset, a large collection of multi-source dermatoscopic images of common pigmented skin lesions. *Scientific data* 5, 1 (2018), 1–9.

[64] Paul Voigt and Axel Von dem Bussche. 2017. The eu general data protection regulation (gdpr). *A Practical Guide*, 1st Ed., Cham: Springer International Publishing (2017).

[65] Kang Wei, Jun Li, Chuan Ma, Ming Ding, Sha Wei, Fan Wu, Guihai Chen, and Thilina Ranabuduge. 2022. Vertical federated learning: Challenges, methodologies and experiments. *arXiv preprint arXiv:2202.04309* (2022).

[66] Yuncheng Wu, Shaofeng Cai, Xiaokui Xiao, Gang Chen, and Beng Chin Ooi. 2020. Privacy preserving vertical federated learning for tree-based models. *arXiv preprint arXiv:2008.06170* (2020).

[67] Jianping Yan, Lifei Wei, Xiansong Qian, and Lei Zhang. 2025. IDPriU: A two-party ID-private data union protocol for privacy-preserving machine learning. *Journal of Information Security and Applications* 88 (2025), 103913.

[68] Andrew Chi-Chih Yao. 1986. How to generate and exchange secrets. In *27th annual symposium on foundations of computer science (Sfcs 1986)*. IEEE, 162–167.

[69] Wenting Zheng, Ankur Dave, Jethro G. Beekman, Raluca Ada Popa, Joseph E. Gonzalez, and Ion Stoica. 2017. Opaque: An Oblivious and Encrypted Distributed Analytics Platform. In *14th USENIX Symposium on Networked Systems Design and Implementation (NSDI 17)*. USENIX Association, Boston, MA, 283–298. <https://www.usenix.org/conference/nsdi17/technical-sessions/presentation/zheng>

APPENDIX

A Supporting Different Data Row Counts

In a real-world scenario, the two parties typically hold input data with different row counts. We introduce a simple method to adapt our proposed **Bifrost** to support varying data count. Let n_a and n_b represent the input data row counts of parties P_a and P_b , respectively. The adaptation method is straightforward: both parties need to generate random permutations and a random matrix that corresponds to the sizes of their respective input data. Specifically, in offline phase of Π_{SMIG} (Protocol 3), P_a samples one random permutation $\pi_1^a : [n_a] \mapsto [n_a]$ and another random permutation $\pi_2^a : [n_b] \mapsto [n_b]$. Meanwhile, P_a samples one random permutation $\pi_1^b : [n_b] \mapsto [n_b]$ and another random permutation $\pi_2^b : [n_a] \mapsto [n_a]$. In addition, in the offline phase of Π_{MI-SFA} (Protocol 4), P_a samples random matrix $R^a \in \mathbb{Z}_{2^\ell}^{n_a \times m_a}$, while P_b samples random matrix $R^b \in \mathbb{Z}_{2^\ell}^{n_b \times m_b}$.

B Security Proof for Theorem 1

THEOREM 1. *The functionality \mathcal{F}_{SMIG} in Figure 4 reveals no information beyond what is revealed by the joined table row count c to both parties.*

PROOF SKETCH. Let \mathcal{A} be a PPT adversary corrupting either P_a or P_b , and let $c = |\text{MIPairs}|$ denote the size of the intersection (i.e., the row count of the joined table). The simulator Sim is given only c . Sim samples two lists of independent, uniformly random values I^1 and I^2 , each of size c , and constructs the set of pairs $\text{MIPairs}^S = [(I_i^1, I_i^2)]_{i \in [c]}$. Sim then outputs MIPairs^S as the simulated view of adversary \mathcal{A} . By the uniform randomness of the unknown permutations π_1 and π_2 from each party, the distribution of each mapped index in MIPairs is uniform and independent. Therefore, the distribution of MIPairs^S is identical to that of MIPairs observed by \mathcal{A} in the execution of \mathcal{F}_{SMIG} . Hence, for any adversary \mathcal{A} , the simulated view is indistinguishable from the real one. \square

C Communication Complexity Comparison

Online communication analyze of **Bifrost.** The online communication cost of **Bifrost** involves 4 rounds and $3n\sigma + 2c\lceil \log_2 n \rceil + nm\ell$ bits, where σ is the bit-length of the ECC private key. The online communication of **Bifrost** consists of two parts: **SMIG** protocol Π_{SMIG} (Protocol 3) and **MI-SFA** protocol Π_{MI-SFA} (Protocol 4).

- The **SMIG** protocol has a communication complexity of 3 rounds and a size of $3n\sigma + 2c\lceil \log_2 n \rceil$ bits. The process begins with P_a sending n encrypted elements to P_b , resulting in $n\sigma$ bits. In the second round, P_b sends two lists of n encrypted elements back to P_a , resulting in $2n\sigma$ bits. In the final round, P_a sends the mapped intersection index pairs to P_b , resulting in $2c\lceil \log_2 n \rceil$ bits, where c is the row count of the joined table.
- The **MI-SFA** protocol has a communication complexity of 1 round and a size of $(m_a + m_b)\ell$, assuming parallel execution of its send and receiving operations. The communication cost is entirely attributed to two concurrent invocations of the $\Pi_{O\text{-Shuffle}}$ sub-protocol. In this round, party P_a sends its $n \times m_a$ masked feature matrix, a total of $nm_a\ell$ bits, while P_b sends its $n \times m_b$ masked feature matrix, a total of $nm_b\ell$ bits.

The SMIG protocol cost is independent of the feature dimensions m and is much smaller than that of the MI-SFA protocol. Consequently, the overall communication of *Bifrost* is dominated by the MI-SFA protocol and scales roughly with the dataset size $n \cdot m$.

Offline communication analyze of *Bifrost*. *Bifrost* requires the shuffled random matrix shares generated by $\Pi_{O\text{-Shuffle}}$ (Algorithm 2 in *iPrivJoin* [40]) to mask the feature data of P_a and P_b , respectively. Therefore, the communication size of our offline phase is $O((\kappa + \lambda)n \log nm)$ bits.

Online communication analyze of *iPrivJoin* [40]. *iPrivJoin* consists of three steps: private data encoding, oblivious shuffle, and private data trimming. In the first step, both parties invoke the OP-PRF on the IDs and features to share P_b 's features. P_a secret shares its feature data. And two parties invoke an OPRF once to encode ID data. Thus, both parties obtain an encoded ID vector and a secret-shared dataset containing aligned features and redundant samples. The communication size for the first step is $O(hn(\lambda + \log n + m_b \kappa) + nm_a \ell)$ bits, and the number of rounds is 8. In the second step, both parties send and receive twice the masked datasets, which results in a communication size of $O(nml + n\kappa)$ and 2 communication rounds. In the final step, the encoded IDs are reconstructed, resulting in the communication size of $O(n\kappa)$, and the number of rounds is 1. Thus, the total communication complexity and the number of rounds for *iPrivJoin* are $O(hn(\lambda + \log n + m_b \kappa) + nml + n\kappa)$ bits and 11, respectively.

Offline communication analyze of *iPrivJoin* [40]. *iPrivJoin* requires the shuffled random matrix shares generated by two times of $\Pi_{O\text{-Shuffle}}$ (Algorithm 2 in *iPrivJoin* [40]) to mask both feature data and ID data from both parties. As a result, the communication size in the offline phase is $O((\omega\kappa + \lambda)n \log(\omega n)m)$ bits.

D Two Protocols for Secure Statistical Analysis

The full protocols we design for the secure Chi-square test (i.e., χ^2 -test) computation and the secure Pearson correlation computation are shown in Protocol 5 and Protocol 6, respectively. Below, we introduce the two protocols.

D.1 Secure Chi-square Test. As shown in Protocol 5, the secure χ^2 -test computation protocol $\Pi_{\chi^2\text{-test}}$ inputs two columns of secret-shared aligned features $\langle X \rangle$ and $\langle Y \rangle$, and outputs a secret-shared χ^2 -test vale $\langle v \rangle$, where $v = \chi^2\text{-test}(X, Y)$. In addition, $CatX$ are the categories of the feature X and $CatY$ are the categories of the feature Y .

The protocol begins by having the parties jointly construct a secret-shared contingency table $\langle ContingencyT \rangle$, where each entry $\langle ContingencyT_{j,k} \rangle$ contains the count of records for which the features correspond to the category pair $(CatX_j \parallel CatY_k)$ (Lines 1-12). Next, the parties compute the secret-shared marginal totals for rows ($\langle ColSum \rangle$) and columns ($\langle RowSum \rangle$) from the contingency table (Lines 13-18). Using these marginals, they then calculate the secret-shared expected frequency table $\langle E \rangle$ under the null hypothesis of independence (Lines 19-20). Using these secret-shared marginals, they then calculate the secret-shared expected frequency table $\langle E \rangle$ under the null hypothesis of independence (Lines 19-20). To mitigate numerical growth, our protocol introduces an optimization: instead of computing the matrix product of the marginals and then

Protocol 5: $\Pi_{\chi^2\text{-Test}}$

Parameters: The categories of the first feature $CatX$; The categories of the second feature $CatY$; The row count of input data n ;

Inputs: Two columns of the secret-shared aligned features $\langle X \rangle$ and $\langle Y \rangle$.

Outputs: A secret-shared $\chi^2\text{-test}$ value $\langle v \rangle$, where $v = \chi^2\text{-test}(X, Y)$

```

1: for  $j = 1$  to  $|CatX|$  in parallel do
2:   for  $k = 1$  to  $|CatY|$  in parallel do
3:      $\langle CatXY_{i,j+k*|CatX|} \rangle = (\langle X_i \parallel Y_i \rangle == CatX_j \parallel CatY_k)$ .
4:   end for
5: end for
6: for  $i = 1$  to  $n$  in parallel do
7:   for  $j = 1$  to  $|CatX|$  in parallel do
8:     for  $k = 1$  to  $|CatY|$  in parallel do
9:        $\langle ContingencyT_{j,k} \rangle = \langle ContingencyT_{j,k} \rangle + \langle CatXY_{i,j+k*|CatX|} \rangle$ .
10:    end for
11:   end for
12: end for
13: for  $i = 1$  to  $|CatX|$  in parallel do
14:   for  $j = 1$  to  $|CatY|$  in parallel do
15:      $\langle ColSum_i \rangle = \langle ColSum_i \rangle + \langle ContingencyT_{i,j} \rangle$ .
16:      $\langle RowSum_j \rangle = \langle RowSum_j \rangle + \langle ContingencyT_{i,j} \rangle$ .
17:   end for
18: end for
19:  $\langle RowSum \rangle = \langle RowSum \rangle / n$ .
20:  $\langle E \rangle = MatMul(\langle ColSum_i \rangle, \langle RowSum \rangle^T)$ .
21:  $\langle v \rangle = Sum((\langle ContingencyT \rangle - \langle E \rangle)^2 / \langle E \rangle)$ 

```

dividing by the total count n , we first divide the $\langle RowSum \rangle$ vector by n (Line 19) before the matrix multiplication (Line 20). This ordering is crucial for computations over finite rings, as it reduces the magnitude of the intermediate values, thereby preventing potential overflows and enabling the use of a smaller ring, which in turn minimizes computational and communication overhead. Finally, the protocol computes the χ^2 -test share $\langle v \rangle$ by securely summing the element-wise squared differences between the observed frequencies in $\langle ContingencyT \rangle$ and the expected frequencies in $\langle E \rangle$, normalized by the expected frequencies (Line 21).

D.2 Secure Pearson Correlation. As shown in Protocol 6, the secure Pearson correlation computation protocol $\Pi_{Pearson}$ inputs two columns of secret-shared aligned features $\langle X \rangle$ and $\langle Y \rangle$, and outputs a secret-shared pearson correlation value $\langle v \rangle$, where $v = Pearson(X, Y)$.

Initially, the parties collaboratively compute the secret-shared means, $\langle X_mean \rangle$ and $\langle Y_mean \rangle$, for each vector (Lines 1-2). Subsequently, they calculate the deviation of each element from its respective mean, producing the secret-shared difference vectors $\langle X_dif \rangle$ and $\langle Y_dif \rangle$ (Lines 3-6). The protocol then proceeds to compute the core components of the Pearson formula: the secret-shared covariance, which is the dot product of the two difference vectors (Line 7), and the sum of squared deviations for each vector, $\langle X_dev \rangle$ and $\langle Y_dev \rangle$ (Lines 8-9). Finally, a crucial optimization in our proposed protocol is avoiding a high-overhead secure division. The standard Pearson formula involves a secure division by the product of standard deviations. Secure division in secret

Table 8: Comparison of Bifrost vs. iPrivJoin [40] across three phases (offline, setup, and online) on eight real-world datasets. Results from the Online phase are highlighted: blue indicates better performance, while gray indicates worse performance. “Education” refers to the Education Career Success dataset.

Dataset		Education	Breast Cancer Gene	Skin Cancer	a9a	ARCENE	MNIST	Tiny ImageNet	CelebA
Time (s)	Setup	Bifrost [40]	0.90 0.02	0.36 0.01	1.93 0.03	5.91 0.20	0.27 0.01	11.55 0.17	24.52 0.38
	Offline	Bifrost [40]	28.35 61.01	923.67 1894.27	1428.97 3017.93	358.01 811.16	11571.50 23396.34	3257.21 7557.74	23697.00 5559.89
		Bifrost [40]	1.17 2.97	1.46 19.37	7.11 108.07	8.24 61.88	6.28 122.78	41.15 639.93	287.37 5557.13
	Online	Bifrost [40]	40.85 103.89	690.57 1689.20	3427.70 8438.50	1810.01 4574.48	5690.00 13831.38	21968.86 55595.27	189022.21 478611.54
		Bifrost [40]	1.21 7.96	10.25 67.44	60.87 385.51	33.98 247.85	68.76 438.45	365.20 2304.43	3135.53 19885.10
	Memory Cost (MB)	Bifrost [40]	19.82 27.83	83.23 217.25	437.18 1142.05	181.54 680.80	493.84 1299.34	2555.14 6830.83	21937.85 58822.61
		Bifrost [40]	1.40× 1.40×	2.61× 2.61×	2.61× 3.75×	2.63× 2.67×	2.68× 2.68×	2.56× 2.56×	53518.57 136947.61

Protocol 6: Π_{Pearson}

Parameters: The row count of input data n ; The bit length of element ℓ .

Inputs: Two columns of the secret-shared aligned features $\langle X \rangle$ and $\langle Y \rangle$.

Outputs: A secret-shared Pearson correlation value $\langle v \rangle$, where $v = \text{Pearson}(X, Y)$.

Online:

- 1: $\langle X_{\text{mean}} \rangle = \text{Sum}(\langle X \rangle) / n$.
- 2: $\langle Y_{\text{mean}} \rangle = \text{Sum}(\langle Y \rangle) / n$.
- 3: **for** $i = 1$ **to** n **in parallel do**
- 4: $\langle X_{\text{dif}}_i \rangle = \langle X_i \rangle - \langle X_{\text{mean}} \rangle$.
- 5: $\langle Y_{\text{dif}}_i \rangle = \langle Y_i \rangle - \langle Y_{\text{mean}} \rangle$.
- 6: **end for**
- 7: $\langle \text{covariance} \rangle = \text{DotProduct}(\langle Y_{\text{dif}} \rangle, \langle X_{\text{dif}} \rangle)$.
- 8: $\langle X_{\text{dev}} \rangle = \text{DotProduct}(\langle X_{\text{dif}} \rangle, \langle X_{\text{dif}} \rangle)$.
- 9: $\langle Y_{\text{dev}} \rangle = \text{DotProduct}(\langle Y_{\text{dif}} \rangle, \langle Y_{\text{dif}} \rangle)$.
- 10: $\langle X_{\text{dev_inv}} \rangle = \text{InvertSqrt}(\langle X_{\text{dev}} \rangle)$.
- 11: $\langle Y_{\text{dev_inv}} \rangle = \text{InvertSqrt}(\langle Y_{\text{dev}} \rangle)$.
- 12: $\langle v \rangle = \langle \text{covariance} \rangle * \langle X_{\text{dev_inv}} \rangle * \langle Y_{\text{dev_inv}} \rangle$.

sharing uses Newton-Raphson’s method for finding a modular inverse, which requires $O(\log(k))$ rounds of multiplication where k is the required precision. Instead, our protocol first computes the secret-shared inverse square roots of $\langle X_{\text{dev}} \rangle$ and $\langle Y_{\text{dev}} \rangle$ (Lines 10-11). This allows the final Pearson correlation coefficient $\langle v \rangle$ to be efficiently computed using only secure multiplications (Line 12), thereby reducing communication rounds and overall overhead.

E Additional Evaluation

E.1 Comparison across Real-World Datasets. As shown in Table 8, we compare Bifrost with iPrivJoin [40] in three phases using eight real-world datasets. The experimental results have been analyzed in the main text and are not further discussed here.

E.2 Comparison on Small-Scale Datasets under Varying Parameters. We conduct evaluations for varying row count n and varying feature dimension m separately.

We conduct experiments on datasets of row count $n \in \{2^{12}, 2^{16}, 2^{20}\}$ with a fixed feature dimension ($m_a = m_b = 100$). As shown in Table 9, Bifrost significantly outperforms the iPrivJoin by $4.17 \sim 10.10 \times$ in running time and $7.43 \sim 7.58 \times$ in communication size. When the dataset is small (e.g., $n = 2^{12}$), our improvements over the iPrivJoin are relatively limited. This is primarily because, under such conditions, both the dataset size and feature dimensionality are low. In this regime, the ECC computation for IDs within our protocol becomes the dominant overhead, thereby creating an efficiency bottleneck. Furthermore, the communication size reduction of Bifrost remains at about 86.63%.

Table 9: Comparison of Bifrost vs. iPrivJoin [40] (feature dimensions $m_a = m_b = 100$) across dataset sizes n .

Protocol	Time (s)			Communication (MB)		
	2^{12}	2^{16}	2^{20}	2^{12}	2^{16}	2^{20}
Bifrost	3.20	19.29	306.12	6.65	106.40	1702.40
iPrivJoin [40]	13.37	194.30	3090.55	50.45	791.03	12653.15

We vary the feature dimensions $m_a = m_b \in \{100, 500, 1000\}$ and fix the dataset row count $n = 2^{16}$. As shown in Table 10, Bifrost outperforms iPrivJoin by $11.85 \sim 17.26 \times$ in terms of running time and $7.43 \sim 7.69 \times$ in terms of communication size. In addition, the performance improvement of Bifrost becomes more pronounced as the feature dimension m increases. For instance, as $m_a = m_b$ increases from 100 to 1000, the running time improvement of Bifrost over iPrivJoin increases from $11.85 \times$ to $17.26 \times$.

E.3 Comparison in Offline Phase. In the offline phase, both Bifrost and iPrivJoin [40] only rely on $\mathcal{F}_{O\text{-}Shuffle}$. iPrivJoin introduces a local extension method to expand the output of $\mathcal{F}_{O\text{-}Shuffle}$ from a single dimension to m dimensions. Although this local extension method improves offline efficiency, it introduces a 1-bit error. As

Table 10: Comparison of Bifrost vs. iPrivJoin [40] (dataset size $n = 2^{16}$) across varying feature dimension m_a and m_b .

Protocol	Time (s)			Communication (MB)		
	100	500	1000	100	500	1000
Bifrost	19.34	53.24	96.26	106.40	506.40	1006.40
iPrivJoin [40]	194.06	951.19	1895.38	791.03	3880.70	7742.78

a result, the extension creates an inaccurately joined table shares, which reduces the accuracy of subsequent SDA tasks. The experimental results on the Skin Cancer dataset in iPrivJoin [40] show a decrease in accuracy due to this error, with accuracy dropping from 88.47% to 88.11%, representing a decrease of approximately 0.41%. Consequently, we use the oblivious shuffle protocol $\Pi_{O\text{-Shuffle}}$ without the extension method to produce precise random values in the offline phase. To ensure a fair comparison, both our protocol and iPrivJoin disable the local extension method and implement the same version of $\Pi_{O\text{-Shuffle}}$ during evaluation.

Table 11: Offline comparison of Bifrost vs. iPrivJoin [40].

Protocol	Time (s)			Communication (MB)		
	2^{12}	2^{16}	2^{20}	2^{12}	2^{16}	2^{20}
Bifrost	27.62	81.98	1016.84	36.31	558.27	10774.62
iPrivJoin [40]	60.30	200.45	2663.15	92.91	1484.26	28513.83

We conduct offline experiments on datasets of varying row count $n \in \{2^{12}, 2^{16}, 2^{20}\}$, with a fixed feature dimension ($m_a = m_b = 10$). As shown in Table 11, Bifrost outperforms the iPrivJoin by an average of $2.42\times$ in terms of time. This significant improvement is primarily due to Bifrost’s enhanced communication complexity, which reduces the communication size by an average of $2.62\times$ compared to the iPrivJoin.

E.4 Comparison with unbalanced secure data join protocol [58]. One special scenario is the unbalanced setting [25, 58], where the row count of the two parties’ datasets differs by at least two orders of magnitude. We conduct experiments with the SOTA secure unbalanced and redundancy-free data join protocol Suda [58]. Let n_a and n_b represent the input data row counts of parties P_a and P_b , respectively. We vary the feature dimensions $m_a = m_b \in \{100, 640\}$ and vary P_a ’s row count $n_a \in \{1024, 2048\}$ when fixing P_b ’s row count $n_b = 2^{20}$. The results in Table 12 show that Bifrost achieves $2.24 \sim 5.04\times$ faster running time compared to Suda. However, this performance gain comes with an increase in communication size. This can be explained by the fact that Suda leverages homomorphic encryption to perform polynomial operations on encrypted ciphertexts. As a result, Suda incurs higher computational costs but benefits from reduced communication overhead.

Table 12: Comparison of Bifrost vs. unbalanced protocol Suda [58].

n_b	n_a	Protocol	$m_a = m_b = 100$		$m_a = m_b = 640$	
			Time (s)	Comm. (MB)	Time (s)	Comm. (MB)
2^{20}	1024	Bifrost	73.71	832.85	443.15	5157.07
		Suda [58]	171.32	154.42	993.57	508.01
2^{20}	2048	Bifrost	73.90	833.70	445.87	5162.14
		Suda [58]	353.81	226.57	2245.70	933.71

F Strengthening the Threat Model

In this section, we elaborate on the path to strengthen the threat model of Bifrost. Bifrost comprises Π_{SMIG} (Protocol 3) and $\Pi_{MI\text{-SFA}}$ (Protocol 4), which are secure against semi-honest adversaries. In contrast to semi-honest adversaries who follow all protocol specifications but passively attempt to learn additional information, malicious adversaries may try to deviate from the protocol to either obtain private information or compromise its functionality. The main challenges in strengthening Bifrost to secure against malicious adversaries are twofold: (i) ensuring that the ECC-based ID encrypting step in Protocol 3 is executed correctly by both parties, as this is the main interactive component; (ii) ensuring that the oblivious shuffle protocol in Protocol 4 is performed correctly, as this is the only interactive process in Protocol 4.

We can strengthen Bifrost against these malicious behaviors by (i) augmenting Π_{SMIG} (Protocol 3) with a commitment scheme [49] and Non-Interactive Zero-Knowledge proofs (NIZKs) [19, 22], and (ii) replacing underlying oblivious shuffle protocol $\Pi_{O\text{-Shuffle}}$ in $\Pi_{MI\text{-SFA}}$ (Protocol 4) with malicious-secure oblivious shuffle protocol in Figure 12 of [59]. Since the latter is a modular, drop-in substitution, we focus below on augmenting Π_{SMIG} (Protocol 3) using the commit-and-prove paradigm.

Zero-knowledge notation. Let $(\mathbb{G}, +)$ be a prime-order cyclic group of order q generated by g . Let $\text{Com}(\cdot; \cdot)$ be a commitment scheme (e.g., instantiated with Pedersen commitments [49]) with standard binding and hiding properties. Let Π_{NIZK} be a NIZK system. For a relation \mathcal{R} , x denotes the public statement, w denotes the corresponding private witness such that $(x, w) \in \mathcal{R}$, and a proof π^{zkp} allows a prover to convince a verifier of the validity of x without leaking any information about w .

Commit phase. First, we introduce a commitment phase before the Setup step in Protocol 3. P_a generates commitments $C_{ID^a} = \text{Com}(ID^a; r_{ID^a})$, $C_{\pi_1^a} = \text{Com}(\pi_1^a; r_{\pi_1^a})$, $C_{\pi_2^a} = \text{Com}(\pi_2^a; r_{\pi_2^a})$, $C_\alpha = \text{Com}(\alpha; r_\alpha)$ (collectively abbreviated as $C_a = \text{Com}(ID^a, \pi_1^a, \pi_2^a, \alpha; R_a)$) to its identifiers, its two permutations, and its private key, using randomness. Similarly, P_b use randomness to generate commitments $C_{ID^b} = \text{Com}(ID^b; r_{ID^b})$, $C_{\pi_1^b} = \text{Com}(\pi_1^b; r_{\pi_1^b})$, $C_{\pi_2^b} = \text{Com}(\pi_2^b; r_{\pi_2^b})$, $C_\beta = \text{Com}(\beta; r_\beta)$ (collectively abbreviated as $C_b = \text{Com}(ID^b, \pi_1^b, \pi_2^b, \beta; R_b)$). Two parties exchange these commitments with communication complexity $O(n)$ for n identifiers. All subsequent NIZKs are proven relative to these commitments, and any verification failure causes an immediate protocol abort.

Adding prove-and-verify in three substeps 1.(1)–1.(3). In Online Step 1-(1), when P_a sends $\alpha H(\pi_1^a(ID^a))$ to P_b , it appends a proof π_1^{zkp} . This proof π_1^{zkp} demonstrates knowledge of the values committed in $C_a = \text{Com}(ID^a, \pi_1^a, \pi_2^a, \alpha; R_a)$ and that $\alpha H(\pi_1^a(ID^a))$ is correctly computed such that $(\alpha H(\pi_1^a(ID^a)))_{\pi_1^a(i)} = \alpha H(ID_i^a)$ for all $i \in [n]$. This proof ensures P_a uses its committed identifiers ID^a , permutation π_1^a and private key α to generate the shuffled and encrypted identifiers. P_b verifies π_1^{zkp} using C_a and the received $\alpha H(\pi_1^a(ID^a))$, aborting if verification fails.

In Step 1-(2), When P_b sends $\beta \alpha H(\pi_1(ID^a))$ and $\beta H(\pi_2^b(ID^b))$, it appends a NIZK proof π_2^{zkp} . This proof demonstrates knowledge of $(ID^b, \pi_1^b, \pi_2^b, \beta; R_b)$ corresponding to C_b such that: (1) $\beta H(\pi_2^b(ID^b))$

is correctly computed with $(\beta H(\pi_2^b(ID^b)))_{\pi_2^b(j)} = \beta H(ID_j^b)$ for all $j \in [n]$ using the committed ID^b , π_2^b , and β ; and (2) $\beta\alpha H(\pi_1(ID^a))$ is correctly computed by applying the committed permutation π_1^b and key β to the received $\alpha H(\pi_1^a(ID^a))$ such that $(\beta\alpha H(\pi_1(ID^a)))_{\pi_1^b(i)} = \beta(\alpha H(\pi_1^a(ID^a)))_i$ for all $i \in [n]$. P_a verifies π_2^{zkp} using C_b , the previously sent $\alpha H(\pi_1^a(ID^a))$, and the received $\beta\alpha H(\pi_1(ID^a))$ and $\beta H(\pi_2^b(ID^b))$, aborting if verification fails.

In Step 1-(3), after P_a decrypts $\beta\alpha H(\pi_1(ID^a))$ using its private key α to obtain $\beta H(\pi_1(ID^a)) = [\alpha^{-1}(x)]_{x \in \beta\alpha H(\pi_1(ID^a))}$, it computes the mapped intersection index pairs MIPairs . When P_a sends the output MIPairs to P_b , it appends a NIZK proof π_3^{zkp} . This

proof demonstrates that: (1) the decryption was performed correctly using the committed α from C_a such that $(\beta H(\pi_1(ID^a)))_i = \alpha^{-1}((\beta\alpha H(\pi_1(ID^a)))_i)$ for all $i \in [n]$, and (2) MIPairs is computed correctly from $\beta H(\pi_1(ID^a))$ and $\beta H(\pi_2^b(ID^b))$ relative to P_a 's commitment C_a , i.e., MIPairs contains exactly the pairs $(i, \pi_2^a(j))$ for all (i, j) where $(\beta H(\pi_1(ID^a)))_i = (\beta H(\pi_2^b(ID^b)))_j$, and no other pairs. P_b verifies π_3^{zkp} using C_a , the previously sent $\beta\alpha H(\pi_1(ID^a))$ and $\beta H(\pi_2^b(ID^b))$, and the received MIPairs , accepting MIPairs as the final output only if verification succeeds. Across three steps 1.(1)–1.(3), all proofs incur $O(n)$ communication overhead for n identifiers.